NASA Technical Memorandum 78611

NASA-TM-78611 19790024034

Low-Cost Inertial Navigation for Moderate-g Missions

Shmuel J. Merhav

September 1979

NASA

National Aeronautics and
Space Administration

NASA Technical Memorandum 78611

Low-Cost Inertial Navigation for Moderate-g Missions

Shmuel J. Merhav, Ames Research Center, Moffett Field, California

National Aeronautics and
Space Administration

Ames Research Center
Moffett Field, California 94035

LIST OF MAIN SYMBOLS

A_x, A_y	gain factors
b_x, b_y	torquer sensitivities
d	gyro drift rate
$\underline{F}$	specific force vector
F_E	east component of specific force
F_N	north component of specific force
F_V	vertical component of specific force
$\underline{G}$	Earth's gravitation
$\underline{g}$	net gravity vector
G	index of geographical coordinate frame
h	altitude
H	angular momentum
I	moment of inertia; identity matrix
J	moment of inertia
K_x, K_y	amplification
ℓ	index of local level coordinate frame
M_x, M_y	torques on x, y axes
n	spin speed of gyro rotor
R	distance of vehicle from center of the Earth
S	Laplace operator
$\underline{T}$	3 × 3 orthogonal transformation matrix
T_x, T_y	torquers on x, y axes
t	time
u	normalized position or velocity divergence

$\underline{V}_G$, $\underline{\dot{V}}_G$	velocity and acceleration in geographical coordinates
V_E	east component of velocity
V_N	north component of velocity
V_V	vertical (downward) component of velocity
X, Y, Z	axes of cartesian coordinate frame
β_x, β_y	gain factors of the GIMU with respect to its x, y axes
Δ, δ	deviation
λ	latitude
ε	angular deviation from local vertical
ϕ, θ, ψ	air frame roll, pitch, and yaw angles
ψ_A, ψ_E, ψ_N	platform orientation errors
$[\phi]_x$	Euler transformation with respect to the x axis
$[\theta]_y$	Euler transformation with respect to tye y axis
$[\psi]_z$	Euler transformation with respect to the z axis
$\underline{\omega}$	angular rate vector
ω_s	Schuler frequency
$\underline{\Omega}_s$	sidereal rate of rotation of the Earth
$\underline{\Omega}_G$	skew symmetric matrix of component of Earth rotation in geographical coordinates
$\underline{\Omega}_b$	skew symmetric matrix of components of body rates in body axes coordinates
σ	standard deviation
τ	time
η, ξ	gimbal pitch and roll angles

ACRONYMS AND ABBREVIATIONS

IMU	Inertial Measurement Unit
GIMU	Gyroscopic Inertial Measurement Unit
SDF	Single-Degree-of-Freedom Gyroscopy
TDF	Two-Degree-of-Freedom Gyroscope
DTR	Dry-Tuned Rotor Gyroscope
AZG	Azimuth Gyro
LEG	Leveling Gyro

LOW-COST INERTIAL NAVIGATION FOR MODERATE-g MISSIONS

Shmuel J. Merhav*

Ames Research Center

SUMMARY

This paper describes a low-cost inertial navigation system (INS) concept for a broad class of flight missions characterized by moderate accelerations and limited attitude variations. Typically, these missions may involve general aviation aircraft, helicopters, or remotely piloted vehicles (RPV). Though highly desirable, the use of inertial navigation in these aircraft might be precluded by the high cost of INS technology constituting a substantial fraction of the total aircraft cost. The significance of the moderate acceleration and limited attitude is reviewed with respect to platform mechanization and instrumentation, and a novel hybrid mechanization, partially gimballed and partially strapdown, is presented. Implemented by an unbalanced two-axis gimbal system, controlled by a two-degree-of-freedom gyro, it provides locally level two-axis acceleration information, along with pitch and roll measurements. Heading information is provided by a second gyro mounted in the inner gimbal. It is shown that the system error model is equivalent to that of a conventional platform with a tilt error determined by the integral of the gyro drift rate and an equivalent accelerometer bias proportional to the same drift angle. Thus, by calibrating platform drift rate, the accelerometer-type errors are also cancelled. Rapid gyrocompassing, implemented with opened gimbal control loops, and a strapdown procedure also provides calibration of gyro drift rate biases. Being subjected to small angular inputs and a low-g environment, g and g^2 dependent errors are negligible. Thus, adequate precision can be obtained from moderate cost gyroscopes, resulting in a rms navigation error of the order of 1 n. mi./hr. The dispensing of accelerometers and the simplified mechanization and computation imply substantial cost savings and improvement of reliability.

I. INTRODUCTION

Autonomous navigation, which by definition excludes external navigation aids, is essentially based on inertial instrumentation, except for the crudest heading and velocity methods using magnetic and airspeed measurements. Originally developed for ballistic missiles and military aircraft with all-attitude and high-g capability, the technology in a state-of-the-art inertial navigation system (INS) of the 1 n. mi./hr class incurs costs in the $50,000-$100,000 range. This high cost often precludes its use in a wide scope of applications

---

*Senior NRC Research Associate. Professor, Department of Aeronautical Engineering, Technion, Haifa, Israel.

such as general aviation, helicopters, RPV's, and ground vehicles. In these applications the principal common factor is their low-g environment. It is the purpose of this paper to show how these relatively benign dynamic conditions can be advantageously used in the choice of sensors and IMU mechanization, so as to achieve a substantial reduction in cost and complexity.

Efforts to reduce cost and size and to improve reliability have, in the past decade, been largely oriented to strapdown mechanizations (ref. 1). However, since by far greater demands are placed on the gyroscopes and on on-board computational volume and speed, the advantages expected from dispensing with the gimbal system are largely offset. The greater sensitivity of strapdown systems to alignment errors (ref. 2) and to correlated noise components in the accelerometers and gyroscopes (ref. 3) have so far impeded their successful competition with gimballed systems in the 1 n. mi./hr class (refs. 1 and 2). For short-term guidance in tactical missiles or in aided navigation with frequent updating (ref. 4), strapdown mechanization is superior with respect to miniaturization and reliability.

Alternative approaches for significant improvement in cost effectiveness appear to involve a major departure from classical inertial navigation principles or an entirely new concept in its instrumentation. Examples of such departures have recently been reported. By constructing an optimal observer (ref. 5) on the (known) parameters of the aircraft, velocities are estimated from measurements of roll rate, pitch rate, heading, and altitude. The method appears to have good potential for short-term autonomous navigation. However, further work is needed with regard to sensitivity to parameter variations, trim errors, and wind modeling. An attempt to depart from conventional IMU instrumentation by entirely dispensing with gyroscopes has recently been reported in reference 6. A single-axis physical pendulum is Schuler tuned by measuring the angular acceleration induced by external specific forces and artificially providing the immense moment of inertia of a Schuler pendulum by a torque motor, driven by the highly amplified angular acceleration signal. Not being gyroscopic, the attractive property of the device is its indifference to the Earth's rotation. However, the excessive gain ($\sim 10^7$) and gain stability required in its realization raises doubts as to its performance in an actual flight environment.

An earlier attempt to depart from conventional IMU instrumentation by dispensing with accelerometers has been reported by Hector (ref. 7) and Astrom and Hector (ref. 8). Instead of a simple pendulum, a gyro-pendulum is Schuler tuned, again requiring excessive torquing commands. Additional angular motion sensors and torquers are however, required to provide platform isolation from vehicular attitude motion. A detailed design and error analysis of this concept has been reported by Koenke (ref. 9), verifying that the system obeys the basic laws of error propagation in INS. The advantage of dispensing with the accelerometers is apparently offset by a large sensitivity to vibration and the need for critical adjustments of the large gains. The foregoing examples, aimed at reducing the cost of the sensor package, reflect the continuing search for low-cost navigation systems, especially for the aforementioned type of low-g missions in the 1 n. mi./hr class for which the technologies of conventional IMU's, originally developed for military applications, are highly overdesigned.

In the IMU configuration presented in this paper, the less demanding low-g environment is exploited so as to achieve a substantial reduction in the number of inertial sensors and in the complexity of mechanization without departing from the basic principles of inertial navigation (ref. 5) or resorting to new instrumentation concepts (ref. 6). It is shown that, with modern strapdown gyros, the gimballed and strapdown concepts can be combined into a hybrid mechanization, using two gimbals only and dispensing with the accelerometers. The local-level, two-axis acceleration information is provided by the two gimbal torquers, pitch and roll measurements by pick-offs, and the heading information by an azimuth gyroscope mounted in the inner gimbal. This hybrid mechanization, requiring only the single azimuth Euler transformation, which can be executed by a conventional, relatively slow microprocessor, has apparently not been considered before. It appears to be superior in cost effectiveness to both the gimballed and strapdown mechanizations.

The feasibility of the method is investigated by modeling the dynamics, controls, and error sources in the sensors and system and by statistical analysis of the error propagation for flight durations of 1 hr. If experimentally validated in the future, the proposed solution might lead to a substantial extension of autonomous navigation to the types of aircraft in which low cost is of paramount importance.

II. SYSTEM CONSIDERATIONS

In this section, INS mechanizations are reviewed in the light of the assumptions and requirements characterizing moderate-g missions. The conclusions point to the hybrid mechanization presented in this paper.

A. Assumptions

The class of mission profiles, for which low-cost autonomous navigation is considered in this report, is characterized as follows:

1. Atmospheric flight at moderate altitudes and velocities typical of general aviation, helicopters, RPV's and surface vehicles.

2. The specific forces acting on the vehicle do not exceed the order of 1 g.

3. Unlimited attitude except in pitch, which is limited to $\sim\pm 80°$, as typical in vehicles controlled by vertical gyroscopes.

4. Yaw rate is assumed not to exceed values on the order of 10°/sec.

5. Navigation is implemented in conventional spherical coordinates, disregarding Earth oblateness.

6. The magnitude and direction of the gravity vector are known constants throughout the flight mission.

7. Duration of a typical autonomous flight phase does not exceed ~1 hr.

8. Altitude information is derived from conventional altimeters (barometric or other).

9. The navigation error defined in the local-level plane during the autonomous flight phase should not exceed the order of 1 n. mi.

B. Review of Mechanization Problems

1. Navigation Equations

The relation between acceleration $\ddot{\underline{R}}$, specific force $\underline{F}$, and gravitation $\underline{G}$ in a reference frame rotating at an angular rate $\underline{\omega}$ with respect to inertial space is

$$\underline{F} + \underline{G} = \ddot{\underline{R}} + \dot{\underline{\omega}} \times \underline{R} + 2\underline{\omega} \times \dot{\underline{R}} + \underline{\omega} \times (\underline{\omega} \times \underline{R}) \tag{1}$$

Expressed in geographic coordinates of a perfectly spherical Earth, equation (1) takes the form of the nonlinear time-varying differential equation

$$\dot{\underline{V}}_G = \underline{F}_G + \underline{g} + \underline{\Gamma}(\underline{V}_G, \underline{\Omega}_s, \lambda, \underline{R}) \tag{2}$$

where $\underline{g}$ is the net gravity vector given by

$$\underline{g} = \begin{bmatrix} 0 \\ 0 \\ g \end{bmatrix} = \underline{G} - \underline{\Omega}_s \times (\underline{\Omega}_s \times \underline{R}) \tag{3}$$

and $\underline{\Gamma}$ is a known vector valued function of $\underline{V}_G$, and the scalar parameters Ω_s, λ, R. Explicitly, equation (2), with equation (3), takes the form (ref. 3):

$$\begin{bmatrix} \dot{V}_N \\ \dot{V}_E \\ \dot{V}_v \end{bmatrix} = \begin{bmatrix} F_N \\ F_E \\ F_v \end{bmatrix} + \begin{bmatrix} 0 \\ 0 \\ g \end{bmatrix} + \begin{bmatrix} -\left(2\Omega_s \sin \lambda + \frac{V_E}{R} \tan \lambda\right)V_E + \frac{V_N V_v}{R} \\ \left(2\Omega_s \sin \lambda + \frac{V_E}{R} \tan \lambda\right)V_N + 2\Omega_s V_v \cos \lambda + \frac{V_E V_v}{R} \\ -2\Omega_s V_E \cos \lambda - \frac{V_N^2 + V_E^2}{R} \end{bmatrix} \tag{4}$$

in which λ is determined from the integration of $\dot{\lambda} = V_N/R$. $\dot{V}_N$, $\dot{V}_E$, $\dot{V}_V$, F_N, F_E, F_V are defined in the local level, north, east, and vertical coordinate frame. Any mechanization of INS requires:

1. Determination of F_N, F_E, F_V.

2. Integration of equation (4).

In view of assumption 8, V_V can be derived from the independent measurement of altitude h, so that equation (4) reduces to the two-dimensional navigation equation, in which V_V is now a time-varying parameter

$$\begin{bmatrix} \dot{V}_N \\ \dot{V}_E \end{bmatrix} = \begin{bmatrix} F_N \\ F_E \end{bmatrix} + \begin{bmatrix} -\left(2\Omega_s \sin\lambda + \frac{V_E}{R}\tan\lambda\right)V_E + \frac{V_N V_V}{R} \\ \left(2\Omega_s \sin\lambda + \frac{V_E}{R}\tan\lambda\right)V_N + 2\Omega_s V_V \cos\lambda + \frac{V_E V_V}{R} \end{bmatrix} \tag{5}$$

Measures of F_N, F_E, are normally obtained from onboard accelerometers mounted in a coordinate frame (X_a, Y_a, Z_a). The measured specific force vector $\underline{F_a} = \mathrm{col}[F_{xa}, F_{ya}, F_{za}]$ must be transformed to yield F_N and F_E. The three fundamental aspects of inertial navigation emerging from equation (5) are

- Instrumentation — by which the specific force vector $\underline{F}$ is measured in an airborne coordinate frame defining $\underline{F_a}$.

- Transformation — by which these measurements are transformed into the desired local-level geographical coordinate system, $\underline{F_G} = \underline{T_{G/a}}\underline{F_a}$.

- Navigational computation — by which equation (5) is integrated to yield V_N, V_E and, by further integration, vehicle position X_G, Y_G.

2. Instrumentation

Specific Force Measurement- In view of assumption 2, the required measurement range is 1 g and by assumption 9, the allowable null point uncertainty should not exceed 100 μg (appendix C). Thus, the dynamic range is of the order of 10^4 instead of 10^5 in military applications, and 10^6 or better in long-range missions such as transatlantic flight or submarines. This reduction in dynamic range is a key feature in the realization of the low cost of the IMU described in the following section.

Platform Orientation Error- Assuming that the orientation errors in gimballed and strapdown mechanizations are equal, the error of the resulting specific force measurement is determined as follows: For unaccelerated motion along the vertical axis $\dot{V}_V = 0$ in equation (4), the specific force vector acting on the vehicle is $\underline{F} = \mathrm{col}[F_N, F_E, -g]$. An orientation error vector $\underline{\Psi} = \mathrm{col}[\psi_A, \psi_E, \psi_N]$ causes the error $\Delta\underline{F_G} = \mathrm{col}[\Delta F_N, \Delta F_E, \Delta F_V]$.

$$\begin{bmatrix} \Delta F_N \\ \Delta F_E \\ \Delta F_V \end{bmatrix} = \begin{bmatrix} 0 & \psi_A & -\psi_E \\ -\psi_A & 0 & \psi_N \\ \psi_E & -\psi_N & 0 \end{bmatrix} \begin{bmatrix} F_N \\ F_E \\ -g \end{bmatrix} = \begin{bmatrix} \psi_A F_E + \psi_E g \\ -\psi_A F_N - \psi_N g \\ \psi_E F_N - \psi_N F_E \end{bmatrix} \tag{6}$$

By equation (5), only ΔF_N, ΔF_E are relevant. Thus, equation (6) is rewritten:

$$\begin{bmatrix} \Delta F_N \\ \Delta F_E \end{bmatrix} = \psi_A \begin{bmatrix} F_E \\ -F_N \end{bmatrix} + g \begin{bmatrix} \psi_E \\ -\psi_N \end{bmatrix} \tag{7}$$

The first term in equation (7) is the <u>distance</u>-related navigation error, proportional to the azimuth error ψ_A. The second term is the <u>time</u>-related navigation error, due to the platform tilt with respect to the local vertical, ψ_E, ψ_N.

Required Performance of Gyroscopes- In view of assumptions 1 and 7, for an aircraft with a ground speed $V = 300$ m/sec, and a flight duration of 1 hr, the range covered is 1080 km. For a 1 n. mi. error, $\psi_A = 0.1°$ can be tolerated. $\dot{\psi}_A = 0.1°/\text{hr}$ would result in an error of 0.5 n. mi. only. $\dot{\psi}_N$ and $\dot{\psi}_E$, however, must not exceed 0.01°/hr as indicated in appendix A. In the gimballed mechanization, the tolerable error in $\dot{\psi}_A$ is thus ~10 times the error in $\dot{\psi}_N$ and $\dot{\psi}_E$. In the strapdown mechanization, however, all three angular rate measurements interact to yield the required direction cosine matrix. Thus, all angular rate measurements must be in the 0.01°/hr class.

Furthermore, the rate input range of the gyros is directly dictated by the attitude rates of the aircraft. As a result, the dynamic range of a strapdown gyro for missions characterized in assumptions 1 through 9 is from 0.01°/hr to 100°/sec, i.e., a dynamic range of 36×10^6, as compared to gimballed platforms in which the required dynamic range is from 0.01°/hr to 10°/hr (i.e., a dynamic range of 10^3). The large input rates in strapdown systems, based on spinning wheel type gyros, incur intensive torquer activity, which causes greater temperature fluctuations and reduced accuracy. Also, the excessive demands on torquer scale-factor accuracy essentially exclude moderate-cost spinning-wheel gyros from strapdown systems, even for the relatively benign mission requirements defined in assumptions 1 through 4.

Alignment and Calibration- A comparison of the effect of gyro and accelerometer alignment error on navigation accuracy for gimballed and strapdown systems is given in reference 2. It is indicated that the analytical leveling in the strapdown mechanization is valid only for the airframe orientation on the ground at which the leveling was performed. In subsequent turns during flight, the computer-derived axis system tilts with respect to the instrument axis system. This effect does not exist in gimballed systems. Gyro axis misalignment also causes by far a larger error in strapdown systems than in gimballed systems. These errors are flight-profile-dependent and cannot easily be detected on the ground. A special fixture for tilting the entire strapdown system through precise angles is required for calibration and to cancel flight-profile-dependent calibration errors.

Sensitivity to Dynamical Environment- The mechanization of $\underline{T}_{G/b}$ is determined by gyro measurements and $\underline{F}_b$ by the accelerometers. Mechanical vibration of the instrument package may exite correlated signals in $\underline{T}_{G/b}$ and $\underline{F}_b$ and cause a bias in $\underline{F}_G$. This susceptability does not actually exist in a gimballed system.

3. Transformation

In the gimballed mechanization with its coordinate frame (X_p, Y_p, Z_p) perfectly aligned with (X_G, Y_G, Z_G), the transformation of $\underline{F}_p = \text{col}[Fxp, Fyp, Fzp]$ to $\underline{F}_G$ is $\underline{T}_{G/a} = T_{G/p} = I$ and ideally $\underline{F}_p = \underline{F}_G$. In view of assumption 3, the mechanization normally requires at least three gimbals.

In the strapdown mechanization, the instrumentation axis frame being the aircraft frame body axis (X_b, Y_b, Z_b), $\underline{F}_b = \text{col}[F_{xb}, F_{yb}, F_{zb}]$, $\underline{T}_{G/a} = \underline{T}_{G/b}$ and

$$\underline{F}_G = \underline{T}_{G/b}\underline{F}_b \tag{8}$$

where

$$\underline{T}_{G/b} = [\phi]_x[\theta]_y[\psi]_z \tag{9}$$

is the nine-component direction cosine transformation matrix. It is self-evident, that due to the all-attitude capability (assumption 3), <u>all three</u> components F_{xb}, F_{yb}, F_{zb} must be measured to determine F_N, F_E. The mechanization providing $\underline{T}_{G/b}$ is obtained from the following differential equation (ref. 3):

$$\dot{\underline{T}}_{G/b} = -\underline{T}_{G/b}\underline{\Omega}_b + \underline{\Omega}_G\underline{T}_{G/b} \tag{10}$$

The skew symmetric 3 × 3 matrix $\underline{\Omega}_b$ consists of elements determined by the three body axis angular rate measurements p, q, and r; the skew symmetric matrix $\underline{\Omega}_G$ consists of the three angular rate elements of the rotating coordinate geographic frame, at the location of the vehicle. It follows that since the angular rate measurements p, q, and r and all three components of $\underline{F}_b$ are required, assumptions 1 through 9 do not permit savings or simplifications in the strapdown mechanization.

4. Computation

In the gimballed mechanization, the computation required is essentially the integration of equation (5). Since the second term consists of comparatively slowly varying parameters and variables and in view of assumptions 1, 2, and 4, they will be three orders of magnitude smaller than the first term, the computation of the second term can be performed at an iteration rate in the range of 1 to 10 Hz. The first term is normally integrated at a 40-Hz iteration rate. In the strapdown mechanization, in addition to integrating equation (5), equation (10) must be integrated and equation (8) must be computed at a normal iteration rate of 40 Hz. Thus, assumptions 1 through 9 do not lead to compromises with regard to computational volume and speed. A comparison of a completely coded navigation program for a strapdown system with a program for a gimballed INS shows that the latter uses 30% of the real-time computer capacity and 30% less memory storage than does the former (ref. 2).

C. Summary

The foregoing comparison of gimballed and strapdown mechanizations, based on low-cost spinning-wheel gyroscopes, clearly indicates the superiority of the former for the class of missions considered in this report. The main conclusions, as they relate to assumptions 1 through 9, are summarized in table I.

D. Rationale for a Hybrid Mechanization

The foregoing system considerations and conclusions explain the limitations of a cost-effective wide spread implementation of a strapdown or a gimballed INS for the class of missions considered here. However, by combining the most essential functions of the gimballed concept (isolation of the leveling gyro) with the least critical function of the strapdown concept (azimuth Euler transformation) into a hybrid mechanization, major savings in cost and complexity can be achieved. This hybridization is made feasible by the limited attitude requirement, the low-g environment, and the availability of strapdown type gyros (large angular rate inputs).

The hybrid mechanization, as described in the next chapter, consists of a two-gimbal system and two gyros only. Acceleration information is provided by the gimbal torquers and heading information from the azimuth gyro which, being mounted in the inner gimbal, is exposed only to the relatively low yaw-rate inputs and still meet the less stringent requirements for ψ as indicated in section II B.

The dispensing with the accelerometers and one gimbal, while essentially retaining the computational simplicity of the gimballed mechanization, constitutes a major saving in cost.

III. DESCRIPTION OF THE GYROSCOPIC NAVIGATION SYSTEM (INS)

A complete qualitative description of the hybrid mechanization and INS integration is given in this section, along with definitions of axis systems and symbols used in the analyses of the next two sections.

A. The Gyroscopic Inertial Measurement Unit (GIMU)

The device, schematically shown in figure 1, consists of the following elements: a leveling gyroscope LEG; an azimuth gyroscope AZG; and a two-axis gimbal system g_i, g_o, with its torquers T_x, T_y, and pick-offs P_ϕ and P_θ. LEG and AZG are assumed to be identical and of the strapdown TDF type. The gimbal assembly is essentially of the type used in conventional vertical gyroscopes with relatively powerful torquers T_x, T_y, low friction synchro-type pick-offs P_ϕ and P_θ, and low friction bearings $b - b'$. The outer gimbal g_o is hinged to the aircraft frame AF by means of the bearings $b - b'$ along the longitudinal body axis X_b. LEG and AZG are mounted in the inner gimbal g_i and together with an optional bob weight W, impart an intentional mass unbalance to the two-axis gimbal system with its center of mass C.G., ℓ cm below the suspension point, that is, the intersection of axes X_{gi}, Y_{gi}. The gimbal axis Z_{gi} tends to align itself with Z_ℓ so that η and ξ tend to zero. The specific force vector $\underline{F}$ is defined here by $F_{x\ell}$, $F_{y\ell}$, $F_{z\ell}$ in the local-level orthogonal coordinate frame X_ℓ, Y_ℓ, Z_ℓ. X_ℓ is defined along the projection of X_b on $OX_\ell Y_\ell$. It is assumed here that $F_{z\ell} = -g$. (This assumption can be removed, as shown in section IV.) $F_{x\ell}$ and $F_{y\ell}$ excite $\dot{\eta}$ and $\dot{\xi}$, which are sensed by the LEG. The corresponding outputs $\dot{\eta}_m$ and $\dot{\xi}_m$ are amplified and integrated in the networks G_y, G_x (detailed in fig. 4). The outputs of G_y and G_x are applied to the gimbal torquers T_x and T_y, counteracting the reaction torques induced by $F_{x\ell}$ and $F_{y\ell}$. With integral control in G_y and G_x, η and ξ essentially are zero in the steady state. The outputs of G_y and G_x are proportional to $F_{x\ell}$ and $F_{y\ell}$, and are denoted by F_{xp}, F_{yp}, respectively. $F_{z\ell}$ does not exert a torque and is not measured. The dynamic range of F_{xp}, F_{yp} is determined by the ratio of the maximum torques available from T_x and T_y to the friction torques T_f in the gimbal bearings. Realistic values of these torques show that a dynamic range of $\sim 10^4$ can be obtained.

The device performs as a two-axis, horizontally stabilized accelerometer independent of vehicle roll ϕ and pitch θ but dependent on ψ. Assuming that the $\psi = \psi_o$ before takeoff is known, any subsequent yaw rate $\dot{\psi}$ sensed by AZG is integrated by $I_{n\psi}$, and ψ is continuously determined. Therefore, this device constitutes a complete IMU and will further on be referred to as the Gyroscopic Inertial Measurement Unit (GIMU). It does not require accelerometers and has only two gimbals. This simplified configuration constitutes significant savings in complexity and cost in comparison to both the gimballed and strapdown mechanizations listed in table I. Since, in view of section II, the accuracy in $\dot{\psi}_m$ is $\sim 0.1°$/hr and since $\dot{\psi}_{max} \cong 10°$/sec, the dynamic range required from the AZG is only 3.6×10^5, which is ~ 100 times smaller than in typical strapdown applications. A low-cost gyro can meet this requirement. From the criteria of section II, the LEG must have a null point stability of 0.01°/hr. However, this gyro essentially operates in a gimballed mode and its required dynamic range is only 10^4. With proper temperature control and g-compensation, the required null stability can apparently be achieved even with a low-cost gyro (appendix E). This problem is treated in section VI.

The pitch (θ) and roll (ϕ) measurements, obtained from P_θ and P_ϕ, are insensitive to acceleration and can be used for flight control and display purposes in a conventional manner.

B. Integration of the GIMU into a Complete INS

With $\underline{F}_p = \mathrm{col}[F_{xp}, F_{yp}]$ and ψ provided by the GIMU, the transformation defined by equation (8) reduces to

$$\underline{F}_G = [\Psi]_z^T \underline{F}_p \tag{11}$$

and is specifically implemented in the navigation computer by:

$$\begin{bmatrix} F_N \\ F_E \end{bmatrix} = \begin{bmatrix} \cos\psi & -\sin\psi \\ \sin\psi & \cos\psi \end{bmatrix} \begin{bmatrix} F_{xp} \\ F_{yp} \end{bmatrix} \tag{12}$$

With F_N, F_E, equation (5) can be integrated to yield V_N and V_E and by further integration, the position X_G and Y_G. The following gyro precession commands, determined in the navigation computer and fed to the gyro torquers, constitute the complete INS:

1. Schuler tuning: $\dot{\eta}_c{}^s$, $\dot{\xi}_c{}^s$ derived from V_N, V_E in terms of body axes, fed to T_η, T_ξ.

2. Earth rate compensation: $\dot{\eta}_c{}^\Omega$, $\dot{\xi}_c{}^\Omega$, $\dot{\psi}_c{}^\Omega$ derived from Ω_s and λ fed to T_η, T_ξ, T_ψ.

3. Compensation of g-dependent gyro drift: Derived from the known g-sensitivity coefficients of the gyros and from the actual values of F_{xp}, F_{yp} fed to T_η, T_ξ, T_ψ.

4. Compensation of drift rate bias: $\dot{\eta}_c{}^d$, $\dot{\xi}_c{}^d$, $\dot{\psi}_c{}^d$, derived from a calibration procedure and fed to T_η, T_ξ, T_ψ.

The foregoing compensations, as treated in detail in section V, indicate that the complete INS based on the GIMU is feasible. The computations involved are straightforward and can be implemented by a conventional microprocessor.

IV. ANALYSIS OF SYSTEM DYNAMICS AND CONTROL

In this section, the mathematical model of the gyro-pendulum assembly shown in figure 1 is developed. The resulting equations of motion are then used in the analysis of the closed loop GIMU.

A. Open-Loop Gyro-Pendulum Dynamics

The LEG and AZG, assumed to be of TDF DTR type, are described in detail in reference 10. Their open-loop transfer functions are equivalent to those of a classical two-axis symmetrical free rotor gyro

$$\theta_x(S) = -\phi_x(S) + \frac{SM_x(S) - M_y(S)\,\frac{H}{I^r}}{I^r S\left[S^2 + \left(\frac{H}{I^r}\right)^2\right]} \tag{13}$$

$$\theta_y(S) = -\phi_y(S) + \frac{M_x(S)\,\frac{H}{I^r} + SM_y(S)}{I^r S\left[S^2 + \left(\frac{H}{I^r}\right)^2\right]} \tag{14}$$

where (x, y, z) is the gyro-casing reference frame, ϕ_x, ϕ_y, the angular inputs, resolved along x and y; θ_x and θ_y, are the angular outputs; that is, deflections of the rotor with respect to the gyro case; M_x and M_y are the torques applied to the rotor, resolved along the gyro case coordinate frame; H is the angular momentum of the rotor; I^r is the moment of inertia of the rotor about its x and y axes. The loop closure of the gyro is implemented by setting

$$M_y(S) = A(S)\theta_x(S) \tag{15}$$

and

$$M_x(S) = -A(S)\theta_y(S) \tag{16}$$

By proper design of the torquing amplifier A(S), the closed-loop transfer functions are essentially

$$\theta_x(S) = -(H/A(S))\dot{\phi}_x(S) \tag{17}$$

and

$$\theta_y(S) = -(H/A(S))\dot{\phi}_y(S) \tag{18}$$

and from equations (15) and (16) the torques are

$$M_y = -H\dot{\phi}_x \tag{19}$$

$$M_x = -H\dot{\phi}_y \tag{20}$$

For the LEG mounted in the inner gimbal in accordance with figure 1, $M_y = -H\dot{\xi}$ and $M_x = -H\dot{\eta}$. The AZG may be mounted with its spin axis colinear with either the X_{gi} or the Y_{gi} axis. Assuming the former, its reaction torque $M_z = -H\dot{\eta}$ is exerted on the complete airframe and has negligible effect. The reaction torque due to the airframe yaw rate $\dot{\psi}$, is $M_y = H\dot{\psi}$ is disregarded in this section in which $\dot{\psi}$ is assumed to be zero. $H\dot{\psi}$ is treated as a torque disturbance in section VI.

The development of the equations of motion of the gimbal system is based on reference 11. For small values of η, ξ, the equations reduce to

$$I\ddot{\xi} + H\dot{\eta} = -W\ell\xi \tag{21}$$

$$J\ddot{\eta} - H\dot{\xi} = -W\ell\eta \tag{22}$$

where:

$$\left.\begin{aligned} I &= I_x{}^r + I_x^{gi} + I_x^{go} \\ J &= I_y{}^r + I_y^{gi} \\ H &= I_z{}^r n \\ I_y{}^r &= I_x{}^r = I^r \end{aligned}\right\} \tag{23}$$

With specific force components $F_{x\ell}$ and $F_{y\ell}$ defined along X_ℓ and Y_ℓ, equations (21) and (22) are modified to include the corresponding inertia torques (see fig. 2 for sign conventions)

$$I\ddot{\xi} + H\dot{\eta} = -m\ell(g\xi - F_{y\ell}) \tag{24}$$

$$J\ddot{\eta} - H\dot{\xi} = -m\ell(g\eta + F_{x\ell}) \tag{25}$$

Dividing equations (24) and (25) by I and J, respectively, we have

$$\ddot{\xi} + a\dot{\eta} = -\mu(g\xi - F_{y\ell}) \tag{26}$$

$$\ddot{\eta} - b\dot{\xi} = -\nu(g\eta + F_{x\ell}) \tag{27}$$

where $a \triangleq H/I$, $b \triangleq H/J$, $\mu \triangleq m\ell/I$, $\nu \triangleq m\ell/J$. Laplace transforming equations (26) and (27) and rearranging results in

$$[(S^2 + \mu g)(S^2 + \nu g) + abS^2]\xi = (S^2 + \nu g)\mu F_{y\ell} - aS\nu F_{x\ell} \tag{28}$$

$$[(S^2 + \mu g)(S^2 + \nu g) + abS^2]\eta = -(S^2 + \mu g)\nu F_{x\ell} + bS\mu F_{y\ell} \tag{29}$$

The characteristic equation is the quartic

$$S^4 + [g(\mu + \nu) + ab]S^2 + \mu\nu g^2 = 0 \tag{30}$$

Its solution is

$$S_{1,2}^2 = -\frac{[g(\mu + \nu) + ab]}{2} \pm \sqrt{\frac{[g(\mu + \nu) + ab]^2}{4} - \mu\nu g^2} \tag{31}$$

It is readily verified that the discriminant in equation (31) is nonnegative. Therefore the two roots are

$$S_1 = \pm j \left\{ \frac{[g(\mu + \nu) + ab]}{2} - \sqrt{\frac{[g(\mu + \nu) + ab]^2}{4} - \mu\nu g^2} \right\}^{1/2} = \pm j\omega_1 \qquad (32)$$

and

$$S_2 = \pm j \left\{ \frac{[g(\mu + \nu) + ab]}{2} + \sqrt{\frac{[g(\mu + \nu) + ab]^2}{4} - \mu\nu g^2} \right\}^{1/2} = \pm j\omega_2 \qquad (33)$$

Equations (32) and (33) indicate an undamped conical oscillation at the two frequencies ω_1 and ω_2. As an example, the following numerical values are assumed

$H = 8$ gcm sec ; $I = 1$ gcm sec^2 ; $J = 0.5$ gcm sec^2 ; $m\ell = 0.5$ g sec^2

Thus, $a = 8$ sec^{-1}; $b = 16$ sec^{-1}; $\mu = 0.5$ cm^{-1}; $\nu = 1$ cm^{-1}; and $g = 981$ cm/sec^2. From equations (31) and (32)

$$\omega_1 = 20.1 \text{ radsec}^{-1}$$

$$\omega_2 = 34.6 \text{ radsec}^{-1} .$$

Expressing equations (28) and (29) in terms of ω_1 and ω_2 and in response to step inputs of $F_{x\ell}$ and $F_{y\ell}$, the solutions for $\xi(S)$ and $\eta(S)$ are

$$\xi(S) = \frac{\mu(S^2 + \nu g)}{S(S^2 + \omega_1{}^2)(S^2 + \omega_2{}^2)} F_{y\ell} - \frac{a\nu}{(S^2 + \omega_1{}^2)(S^2 + \omega_2{}^2)} F_{x\ell} \qquad (34)$$

$$\eta(S) = - \frac{\nu(S^2 + \mu g)}{S(S^2 + \omega_1{}^2)(S^2 + \omega_2{}^2)} F_{x\ell} = \frac{b\mu}{(S^2 + \omega_1{}^2)(S^2 + \omega_2{}^2)} F_{y\ell} \qquad (35)$$

The solution in time domain is

$$\xi(t) = (\omega_2{}^2 - \omega_1{}^2)^{-1} \left[\mu F_{y\ell} \left(\frac{\nu g - \omega_1{}^2}{\omega_1{}^2} + \frac{\nu g - \omega_2{}^2}{\omega_2{}^2} \right) - \mu F_{y\ell} \left(\frac{\nu g - \omega_1{}^2}{\omega_1{}^2} \cos \omega_1 t \right.\right.$$

$$\left.\left. + \frac{\nu g - \omega_2{}^2}{\omega_2{}^2} \cos \omega_2 t \right) - a\nu F_{x\ell} \left(\frac{\sin \omega_1 t}{\omega_1} + \frac{\sin \omega_2 t}{\omega_2} \right) \right] \qquad (36)$$

and

$$\eta(t) = (\omega_2^2 - \omega_1^2)^{-1}\left[-\nu F_{x\ell}\left(\frac{\mu g - \omega_1^2}{\omega_1^2} + \frac{\mu g - \omega_2^2}{\omega_2^2}\right) + \nu F_{x\ell}\left(\frac{\mu g - \omega_1^2}{\omega_1^2}\cos \omega_1 t\right.\right.$$

$$\left.\left. + \frac{\mu g - \omega_2^2}{\omega_2^2}\cos \omega_2 t\right) + b\mu F_{y\ell}\left(\frac{\sin \omega_1 t}{\omega_1} + \frac{\sin \omega_2 t}{\omega_2}\right)\right] \tag{37}$$

In the ξ, η phase plane, equations (36) and (37) represent a two-mode elliptical trajectory at frequencies ω_1 and ω_2 crossing the origin and having the mean values $\bar{\xi}$ and $\bar{\eta}$

$$\bar{\xi} = \frac{\mu}{(\omega_2^2 - \omega_1^2)}\left[\nu g\left(\frac{1}{\omega_1^2} + \frac{1}{\omega_2^2}\right) - 2\right]F_{y\ell} \tag{38}$$

$$\bar{\eta} = -\frac{\nu}{(\omega_2^2 - \omega_1^2)}\left[\mu g\left(\frac{1}{\omega_1^2} + \frac{1}{\omega_2^2}\right) - 2\right]F_{x\ell} \tag{39}$$

Equations (38) and (39) show that the sensitivities of $\bar{\xi}$ and $\bar{\eta}$ to $F_{y\ell}$ and $F_{x\ell}$ are not equal. A qualitative representation of the solution, equations (36) and (37), is shown in figure 3.

In the foregoing analysis of the pendulum dynamics, frictional damping has been disregarded. Its effect is qualitatively indicated by the dotted trajectory in figure 3.

In the absence of $F_{x\ell}$ and $F_{y\ell}$, a similar elliptical coning motion with its center at the origin, O, would occur. It is determined by setting to zero the right-hand side of equations (28) and (29) and determining the initial conditions $\xi(0)$, $\dot{\xi}(0)$, . . ., and $\eta(0)$, $\dot{\eta}(0)$ . . . .

B. Closed-Loop Analysis

The loop closure of the pendulum is schematically described in figure 1. If $\dot{\xi}_d$ and $\dot{\eta}_d$ denote the unknown drift rates of the LEG, then the outputs are

$$\left.\begin{aligned}\dot{\xi}_m &= \dot{\xi} - \dot{\xi}_d \\ \dot{\eta}_m &= \dot{\eta} - \dot{\eta}_d\end{aligned}\right\} \tag{40}$$

Considering initial tilt angles ξ_i and η_i, the closed-loop equations, by equations (24) and (25) are

$$I\ddot{\xi} + H\dot{\eta} = -m\ell[g(\xi + \xi_i) - F_{y\ell}] - G_x b_x \xi_m \tag{41}$$

$$J\ddot{\eta} - H\dot{\xi} = -m\ell[g(\eta + \eta_i) + F_{x\ell}] - G_y b_y \dot{\eta}_m \tag{42}$$

b_x and b_y are the torque coefficients of the gimbal torquers T_x, T_y. In order to implement integral control, G_x, G_y are:

$$G_x = K_{x_1} + K_{x_2} \int dt + K_{x_3} \iint dt'\ dt \tag{43}$$

$$G_y = K_{y_1} + K_{y_2} \int dt + K_{y_3} \iint dt'\ dt \tag{44}$$

Substituting equations (40), (43), and (44) into equations (41) and (42) dividing through by I, J, respectively, Laplace transforming and rearranging, the solutions of $\xi(S)$ and $\eta(S)$ are

$$\xi(S) = \frac{X(S)\Delta_y(S) - S^2 aY(S)}{\Delta_x(S)\Delta_y(S) + abS^4} \tag{45}$$

$$\eta(S) = \frac{Y(S)\Delta_x(S) + S^2 bX(S)}{\Delta_x(S)\Delta_y(S) + abS^4} \tag{46}$$

where

$$X(S) \triangleq S(\mu F_{y\ell} - \mu g\xi_i) + (A_{x_1}S^2 + A_{x_2}S + A_{x_3})\dot{\xi}_d/S \tag{47}$$

$$Y(S) \triangleq S(-\nu F_{x\ell} - \nu g\eta_i) + (A_{y_1}S^2 + A_{y_2}S + A_{y_3})\dot{\eta}_d/S \tag{48}$$

$$\Delta_x(S) \triangleq S^3 + A_{x_1}S^2 + (A_{x_2} + \mu g)S + A_{x_3} \tag{49}$$

$$\Delta_y(S) \triangleq S^3 + A_{y_1}S^2 + (A_{y_2} + \nu g)S + A_{y_3} \tag{50}$$

$$A_{x_i} \triangleq K_{x_i}b_x/I \ ; \qquad i = 1, 2, 3 \tag{51}$$

$$A_{y_i} \triangleq K_{y_i}b_y/J \ ; \qquad i = 1, 2, 3 \tag{52}$$

Since A_{x_i}, A_{y_i} are large compared with a and b, the sixth order expressions (45) and (46) simplify to

$$\xi(S) = \frac{X(S)}{\Delta_x(S)} = \frac{S\mu(F_{y\ell} - g\xi_i) + A_{x_1}S^2 + A_{x_2}S + A_{x_3})\dot{\xi}_d/S}{S^3 + A_{x_1}S^2 + (A_{x_2} + \mu g)S + A_{x_3}} \tag{53}$$

$$\eta(S) = \frac{Y(S)}{\Delta_y(S)} = \frac{-S\nu(F_{x\ell} + g\eta_i) + (A_{y_1}S^2 + A_{y_2}S + A_{y_3})\dot{\eta}_d/S}{S^3 + A_{y_1}S^2 + (A_{y_2} + \nu g)S + A_{y_3}} \tag{54}$$

Since $\dot{\xi}_d$ and $\dot{\eta}_d$ are assumed to be slow processes, equations (53) and (54) reduce to the following for $S \to 0$:

$$\xi(t) \cong \int \dot{\xi}_d \, dt \tag{55}$$

$$\eta(t) = \int \dot{\eta}_d \, dt \tag{56}$$

That is, the gimbal system tracks the LEG gyro tilt drift angles, as expected.

The outputs from G_x and G_y, that is, the torquing signals of T_x and T_y are

$$m_x = G_x\dot{\xi}_m = G_x(\dot{\xi} - \dot{\xi}_d) \tag{57}$$

$$m_y = G_y\dot{\eta}_m = G_y(\dot{\eta} - \dot{\eta}_d) \tag{58}$$

Differentiating $\xi(S)$ and $\eta(S)$ in equations (53) and (54), substituting the result into equations (57) and (58), rearranging and substituting K_{x_i} and K_{y_i} from equations (51) and (52), the results are

$$m_x = \frac{I}{b_x}\frac{A_{x_1}S^2 + A_{x_2}S + A_{x_3}}{S^3 + A_{x_1}S^2 + (A_{x_2} + \mu g)S + A_{x_3}}[\mu F_{y\ell} - \mu g\xi_i - \mu g\dot{\xi}_d/S - S\dot{\xi}_d] \tag{59}$$

$$m_y = \frac{J}{b_y}\frac{A_{y_1}S^2 + A_{y_2}S + A_{y_3}}{S^3 + A_{y_1}S^2 + (A_{y_2} + \nu g)S + A_{y_3}}[-\nu F_{y\ell} - \nu g\eta_i - \nu g\dot{\eta}_d/S - S\dot{\eta}_d] \tag{60}$$

With knowledge of the nominal values I_n, J_n, and b_{xn}, b_{yn}, the measured specific forces F_{yp} and F_{xp} for $S \to 0$ are defined by $F_{yp} = m_x b_{x_n}/I_n$ and $F_{xp} = m_y b_{y_n}/J_n$. Specifically,

$$F_{yp} = \beta_y(F_{y\ell} - g\xi_i - g\dot{\xi}_d/S) \tag{61}$$

$$F_{xp} = \beta_x(F_{x\ell} + g\eta_i + g\dot{\eta}_d/S) \tag{62}$$

The coefficients $\beta_y = (I/b_x)(b_{x_n}/I_n)$ and $\beta_x = (J/b_y)(b_{y_n}/J_n)$ ideally are equal to unity.

The closed-loop system, thus, is equivalent to two orthogonal accelerometers with scale factor errors $1 - \beta_x$ and $1 - \beta_y$, mounted on a platform with the initial tilt errors ξ_i and η_i and the corresponding tilt drift errors $\dot{\xi}_d/S$ and $\dot{\eta}_d/S$. It is a unique property of this platform that accelerometer bias or alignment errors are nonexistent, since the instrumentation error stems from the single source $\dot{\xi}_d$, $\dot{\eta}_d$.

Typical values for A_{x_1}, A_{x_2}, and A_{x_3}, yielding closed-loop poles at $\omega_{1,2} = -30 \pm 30j$ and $\omega_3 = -40$ for $\mu g = 0.5\times981 = 490$ are: $A_{x_1} = 100$, $A_{x_2} = 2{,}810$, and $A_{x_3} = 36{,}000$. Similarly, for the same closed-loop poles, for $\nu g = 1\times981$, $A_{y_1} = 100$, $A_{y_2} = 2{,}320$, $A_{y_3} = 36{,}000$.

These values provide a bandwidth of ~5 Hz, which is adequate for inertial navigation.

A block diagram describing the closed-loop system is shown in figure 4. In it, the transfer functions in the gyro-pendulum assembly, as derived from equations (28) to (35), are given by

$$\dot{\xi}(S) = \frac{\mu S(S^2 + \nu g)}{(S^2 + \omega_1{}^2)(S^2 + \omega_2{}^2)} F_{y\ell} - \frac{a\nu S^2}{(S^2 + \omega_1{}^2)(S^2 + \omega_2{}^2)} F_{x\ell} \tag{63}$$

$$\dot{\eta}(S) = -\frac{\nu s(S^2 + \mu g)}{(S^2 + \omega_1{}^2)(S^2 + \omega_2{}^2)} F_{x\ell} + \frac{b\mu S^2}{(S^2 + \omega_1{}^2)(S^2 + \omega_2{}^2)} F_{y\ell} \tag{64}$$

The switches S_x and S_y in the torquing loops are explained in section V.

V. SCHULER TUNING, GYROCOMPASSING, AND CALIBRATION

A. Implementation of Schuler Tuning

Schuler tuning is assured by applying the required precession commands $\dot{\xi}_c{}^s$ and $\dot{\eta}_c{}^s$ to the torquers T_ξ and T_η of the LEG. These commands are obtained from $\dot{\xi}_E = V_E/R$ and $\dot{\eta}_N = -V_N/R$, respectively (see fig. 5a), where V_E and V_N are determined by the solution of equation (5). $\dot{\xi}_c{}^s$ and $\dot{\eta}_c{}^s$ must be implemented in the X_ℓ, Y_ℓ, Z_ℓ coordinate frame, shown on the horizontal projection in figure 5(b). The corresponding transformed components are

$$\begin{bmatrix} \dot{\eta}^s \\ \dot{\xi}^s \end{bmatrix} = \begin{bmatrix} \cos\psi & -\sin\psi \\ \sin\psi & \cos\psi \end{bmatrix} \begin{bmatrix} -V_N/R \\ V_E/R \end{bmatrix} \tag{65}$$

and by setting $\dot{\eta}_c{}^s = \dot{\eta}^s$, $\dot{\xi}_c{}^s = \dot{\xi}^s$, the required precession is implemented.

For the short-time and moderate-speed missions considered here as defined in section II, the analysis of the Schuler tuning can be based on the approximation that the second term on the right-hand side of equation (5) is negligible (ref. 12), that is,

$$\left.\begin{aligned}\dot{V}_N &\cong F_N\\ \dot{V}_E &\cong F_E\end{aligned}\right\} \tag{65}$$

Thus, small amplitude components at the sidereal frequency Ω_s are disregarded. V_N and V_E are obtained by integrating equation (12). In accordance with equation (7), the tilt angles $\eta°$ and $\xi°$ are substituted for ψ_E and ψ_N in the X_ℓ, Y_ℓ, Z_ℓ frame, so that the measured specific forces F_{xp} and F_{yp} in equation (12) are

$$F_{xp} = F_{x\ell} + g\eta° \tag{67}$$

and

$$F_{yp} = F_{y\ell} - g\xi° \tag{68}$$

where, in accordance with equations (61) and (62),

$$\eta° \triangleq \eta_i + \dot{\eta}_d/S \tag{69}$$

and

$$\xi° \triangleq \xi_i + \dot{\xi}_d/S \tag{70}$$

It is assumed here that $\beta_x = \beta_y = 1$.

From equations (65), (67), and (68) the required precession rates in the X_ℓ, Y_ℓ, Z_ℓ axis frame are

$$\begin{bmatrix}\dot{\eta}^s\\ \dot{\xi}^s\end{bmatrix} = \frac{1}{R}\begin{bmatrix}\cos\psi & -\sin\psi\\ \sin\psi & \cos\psi\end{bmatrix}\int\begin{bmatrix}\cos\psi & -\sin\psi\\ \sin\psi & \cos\psi\end{bmatrix}\begin{bmatrix}F_{xp}\\ F_{yp}\end{bmatrix}dt \tag{71}$$

The analysis of equation (71) must be performed in geographical coordinates, namely

$$\begin{bmatrix}-\dot{\eta}_N\\ \dot{\xi}_E\end{bmatrix} = \frac{1}{R}\int\begin{bmatrix}\cos\psi & -\sin\psi\\ \sin\psi & \cos\psi\end{bmatrix}\begin{bmatrix}F_{xp}\\ F_{yp}\end{bmatrix}dt \tag{72}$$

With torquing commands applied to T_ξ and T_η, F_{yp} and F_{xp} are determined with respect to the rotating local vertical, that is,

$$F_{xp} = F_{x\ell} + g\eta^{\circ} + g(\eta - \dot{\eta}_c{}^s/S) \tag{73}$$

and

$$F_{yp} = F_{y\ell} - g\xi^{\circ} - g(\xi - \dot{\xi}_c{}^s/S) \tag{74}$$

Substituting equations (73) and (74) into equation (72) and performing the Euler transformation, equation (65) yields $\dot{\eta}_N = -V_N/R$ and $\dot{\xi}_E = V_E/R$, we have

$$-\dot{\eta}_N = \frac{1}{R}\left(\int F_N\, dt + g\int \eta_N^{\circ}\, dt + g\int \eta_N\, dt + g\iint \frac{V_N}{R}\, dt'\, dt\right) \tag{75}$$

and

$$\dot{\xi}_E = \frac{1}{R}\left(\int F_E\, dt - g\int \xi_E^{\circ}\, dt - g\int \xi_E\, dt + g\iint \frac{V_E}{R}\, dt'\, dt\right) \tag{76}$$

In the last expression the small angles ξ and η (dropping indices) are treated as vectors, so that

$$\left.\begin{aligned} \eta_N &= \eta \cos\psi + \xi \sin\psi \\ -\xi_E &= -\eta \sin\psi + \xi \cos\psi \end{aligned}\right\} \tag{77}$$

Laplace transforming and rearranging equations (75) and (76) gives, in view of the approximation of equation (66),

$$S\eta_N = -\frac{V_N}{R} - \frac{g}{RS}\eta_N^{\circ} - \frac{g}{RS}\eta_N - \frac{g}{R^2}\frac{V_N}{S^2} \tag{78}$$

$$S\xi_E = \frac{V_E}{R} - \frac{g}{RS}\xi_E^{\circ} - \frac{g}{RS}\xi_E + \frac{g}{R^2}\frac{V_E}{S^2} \tag{79}$$

The solutions for η_N and ξ_E are, with $g/R \triangleq \omega_s{}^2$,

$$\eta_N(S) = -\frac{\omega_s{}^2}{S^2 + \omega_s{}^2}\eta_N^{\circ} - \frac{V_N}{RS} \tag{80}$$

$$\xi_E(S) = -\frac{\omega_s{}^2}{S^2 + \omega_s{}^2}\xi_E^{\circ} + \frac{V_E}{RS} \tag{81}$$

Equations (80) and (81) reveal the familiar sinusoidal Schuler frequency oscillation due to η_N° and ξ_N° and the rotation resulting from vehicular velocities V_N and V_E. η_N° and ξ_E° are functions of ψ, since they originate from errors in the X_ℓ, Y_ℓ, Z_ℓ axes. Thus, changes in ψ during flight "modulate" the random process $\dot{\xi}_d$ and $\dot{\eta}_d$, so that the error propagation also depends on the actual flightpath.

The actual specific force components, F_N, F_E, in geographical coordinates, are obtained by transforming equations (73) and (74) into geographical coordinates, using equation (66) and substituting equations (80) and (81)

$$F_N = \dot{V}_N + g\eta_N^\circ + g\left(-\frac{\omega_s^2}{S^2 + \omega_s^2}\,\eta_N^\circ - \frac{V_N}{RS} + \frac{V_N}{RS}\right) = \dot{V}_N + g\,\frac{S^2}{S^2 + \omega_s^2}\,\eta_N^\circ \qquad (82)$$

$$F_E = \dot{V}_E - g\xi_E^\circ - g\left(-\frac{\omega_s^2}{S^2 + \omega_s^2}\,\xi_E^\circ + \frac{V_E}{RS} - \frac{V_E}{RS}\right) = \dot{V}_E - g\,\frac{S^2}{S^2 + \omega_s^2}\,\xi_E^\circ \qquad (83)$$

The description of the Schuler tuning implementation is incorporated in figure 6.

B. Gyrocompassing

The mass unbalance of the gyro pendulum is advantageously used to achieve rapid gyrocompassing. On the ground, with the switches S_x, S_y (as shown in fig. 4) open, the pendulum theoretically aligns itself with the local vertical, as predicted by equations (36) and (37) with $F_{x\ell} = F_{y\ell} = 0$. The deviation from true vertical is determined by two factors: 1) the friction torques of the gimbal bearings, and 2) the reaction torques of the gyros due to Ω_s.

1. For a typical bearing friction torque of $T_f = 0.05$ g cm and a mass unbalance of $W\ell = 200$ g cm, the deviation $\Delta\xi$ or $\Delta\eta$ is

$$\Delta\xi \cong \Delta\eta = \frac{T_f}{W\ell} = \frac{0.05}{200} = 250\ \mu\text{rad} \qquad (84)$$

2. The reaction torques exerted on the gimbal system by the LEG and AZG, due to the Earth rate components $\Omega_s \cos\lambda$ and $\Omega_s \sin\lambda$, respectively, are nearly equal at moderate latitudes ($\lambda \sim 45°$) and amount to ~10°/hr. For an angular momentum of the gyros where $H = 8$ g cm sec, the total reaction torque is

$$T_r = \frac{2 \times 8 \times 10}{3600 \times 57.3} \cong 8 \times 10^{-4}\ \text{g cm}$$

This is negligible in comparison with the friction torque and can be disregarded. The precision requirement in azimuth measurement is determined as follows: At a heading angle ψ, the Earth rate components in the X_ℓ, Y_ℓ, Z_ℓ frame are

$$\begin{bmatrix} \Omega_{sx\ell} \\ \Omega_{sy\ell} \\ \Omega_{sz\ell} \end{bmatrix} = \begin{bmatrix} \cos\psi & \sin\psi & 0 \\ -\sin\psi & \cos\psi & 0 \\ 0 & 0 & 1 \end{bmatrix} \begin{bmatrix} \Omega_s \cos\lambda \\ 0 \\ \Omega_s \sin\lambda \end{bmatrix} = \begin{bmatrix} \cos\psi \quad \Omega_s \cos\lambda \\ -\sin\psi \quad \Omega_s \cos\lambda \\ \Omega_s \sin\lambda \end{bmatrix} \tag{85}$$

As a result of the orientation error vector col $[\Delta\xi, \Delta\eta, \Delta\psi]$, the errors in sensing the Earth rate components are

$$\begin{bmatrix} \Delta\dot{\xi} \\ \Delta\dot{\eta} \\ \Delta\dot{\psi} \end{bmatrix} = \begin{bmatrix} 0 & \Delta\psi & -\Delta\eta \\ -\Delta\psi & 0 & \Delta\xi \\ \Delta\eta & -\Delta\xi & 0 \end{bmatrix} \begin{bmatrix} \cos\psi \quad \Omega_s \cos\lambda \\ -\sin\psi \quad \Omega_s \cos\lambda \\ \Omega_s \sin\lambda \end{bmatrix} = \begin{bmatrix} -\Delta\psi \sin\psi \quad \Omega_s \cos\lambda - \Delta\eta\Omega_s \sin\lambda \\ -\Delta\psi \cos\psi \quad \Omega_s \cos\lambda + \Delta\xi\Omega_s \sin\lambda \\ \Delta\eta \cos\psi \quad \Omega_s \cos\lambda + \Delta\xi \sin\psi\Omega_s \cos\lambda \end{bmatrix} \tag{86}$$

In view of equation (84), and since $\Omega_s \sin\lambda$ and $\Omega_s \cos\lambda$ are of the order of 10°/hr, the elements multiplying $\Delta\eta$ or $\Delta\xi$ are of the order of 0.0025°/hr (or less) and can be neglected. The remaining terms are essentially

$$\begin{bmatrix} \Delta\dot{\xi} \\ \Delta\dot{\eta} \\ \Delta\dot{\psi} \end{bmatrix} \cong \begin{bmatrix} -\Delta\psi \sin\psi \quad \Omega_s \cos\lambda \\ -\Delta\psi \cos\psi \quad \Omega_s \cos\lambda \\ 0 \end{bmatrix} \tag{87}$$

The largest tolerable errors $\Delta\dot{\xi}$, $\Delta\dot{\eta}$ in the 1 n. mi./hr class is 0.01°/hr. Thus, from equation (87)

$$\Delta\psi \cong \frac{0.01°/\text{hr}}{10°/\text{hr}} = 0.001 \text{ rad} = 0.057°$$

Therefore, gyrocompassing must be accomplished with a precision of at least 0.057°.

The longitudinal aircraft axis on the ground deviates from the geographical north by the unknown angle ψ. The measured rate outputs of the LEG are then

$$\begin{bmatrix} \dot{\xi}_m \\ \dot{\eta}_m \end{bmatrix} = \begin{bmatrix} \cos\psi & \sin\psi \\ -\sin\psi & \cos\psi \end{bmatrix} \begin{bmatrix} \Omega_s \cos\lambda \\ 0 \end{bmatrix} - \begin{bmatrix} \dot{\xi}_d \\ \dot{\eta}_d \end{bmatrix} = \begin{bmatrix} \cos\psi \\ -\sin\psi \end{bmatrix} \Omega_s \cos\lambda - \begin{bmatrix} \dot{\xi}_d \\ \dot{\eta}_d \end{bmatrix} \tag{88}$$

The values for $\dot{\xi}_m$ and $\dot{\eta}_m$ are fed to a resolver with a variable input angle ψ_i as indicated in figure 6. The resolved outputs $\dot{\xi}_R$ and $\dot{\eta}_R$ are

$$\begin{bmatrix} \dot{\xi}_R \\ \\ \dot{\eta}_R \end{bmatrix} = \begin{bmatrix} \cos(\psi - \psi_i) - \cos \psi_i(\dot{\xi}_d/\Omega_s \cos \lambda) + \sin \psi_i(\dot{\eta}_d/\Omega_s \cos \lambda) \\ \\ -\sin(\psi - \psi_i) - \cos \psi_i(\dot{\eta}_d/\Omega_s \cos \lambda) - \sin \psi_i(\dot{\xi}_d/\Omega_s \cos \lambda) \end{bmatrix} \Omega_s \cos \lambda \tag{89}$$

ψ_i is varied until $\dot{\eta}_R = 0$, so

$$\sin(\psi - \psi_i) \cong \psi - \psi_i = \Delta\psi = -\sin \psi_i(\dot{\xi}_d/\Omega_s \cos \lambda) - \cos \psi_i(\dot{\eta}_d/\Omega_s \cos \lambda) \tag{90}$$

Denoting $\dot{\xi}_d/\Omega_s \cos \lambda \triangleq a$; $\dot{\eta}_d/\Omega_s \cos \lambda \triangleq b$; and $a/(a^2 + b^2)^{1/2} \triangleq \cos \alpha$; $b/(a^2 + b^2)^{1/2} \triangleq \sin \alpha$ we have

$$\sin(\psi - \psi_i) = -(\sin \psi_i \cos \alpha + \cos \psi_i \sin \alpha)(a^2 + b^2)^{1/2}$$

$$= -\sin(\psi_i + \alpha)(a^2 + b^2)^{1/2} \tag{91}$$

Example:

$$a = 0.03°/\text{hr}/10°/\text{hr} = 0.003$$

$$b = 0.02°/\text{hr}/10°/\text{hr} = 0.002$$

$$(a^2 + b^2)^{1/2} = 0.0036$$

$$\cos \alpha = 3/3.6 = 0.833; \ \alpha = 33.55°$$

From equation (91)

$$\sin(\psi - \psi_i) \cong \Delta\psi = -\sin(\psi_i + 33.55°) \times 3.6\times10^{-3}$$

This dependence of $\Delta\psi$ on ψ_i for $-180° \leq \psi_i \leq 180°$ is shown in figure 7. It shows that $\Delta\psi$ can be as large as 0.2°, which exceeds the limitation in equation (87). However, the top row in equation (89) can be used to determine $\Delta\psi$, that is,

$$\dot{\xi}_R = [\cos(\psi - \psi_i) - \cos \psi_i(\dot{\xi}_d/\Omega_s \cos \lambda) + \sin \psi_i(\dot{\eta}_d/\Omega_s \cos \lambda)]\Omega_s \cos \lambda \tag{92}$$

In the example, $\psi - \psi_i = 0.2°$. Assuming an even more conservative error, $\psi - \psi_i = 1°$; $\cos(\psi - \psi_i) = 0.99985$. By subtracting the known value $\Omega_s \cos \lambda$, the residual due to the first term is

$$\cos(\psi - \psi_i)\Omega_s \cos \lambda - \Omega_s \cos \lambda = -\Omega_s \cos \lambda \times 0.00015 = -10°/\text{hr} \times 0.00015$$

$$= -0.0015°/\text{hr}$$

which is negligible. The remaining terms in equation (92) are, after normalization by $\Omega_s \cos \lambda$

$$e = \frac{\dot{\xi}_R - \Omega_s \cos \lambda}{\Omega_s \cos \lambda} = -\cos \psi_i(\dot{\xi}_d/\Omega_s \cos \lambda) + \sin \psi_i(\dot{\eta}_d/\Omega_s \cos \lambda) \qquad (93)$$

Using the same notations as before, we have

$$e = -(\cos \psi_i \cos \alpha - \sin \psi_i \sin \alpha)(a^2 + b^2)^{1/2} \qquad (94)$$

By causing a perturbation $\delta\psi_i$ on ψ_i (e.g., a sine wave of known amplitude), we have

$$\delta e = (\sin \psi_i \cos \alpha + \cos \psi_i \sin \alpha)(a^2 + b^2)^{1/2}\delta\psi_i \qquad (95)$$

But from equation (91), it follows that

$$\delta e = \Delta\psi\delta\psi_i \qquad (96)$$

and

$$\Delta\psi = \frac{\delta e}{\delta\psi_i} \qquad (97)$$

$\Delta\psi$ thus determined is added to the value of ψ_i, which nulls $\dot{\eta}_R$ in accordance with equation (90). The new value $\psi_i + \Delta\psi = \psi_i{}^*$ is now applied to the resolver, which now yields

$$\begin{bmatrix} \dot{\xi}_R{}^* \\ \\ \dot{\eta}_R{}^* \end{bmatrix} = \begin{bmatrix} \cos(\psi - \psi_i{}^*) - \cos \psi_i{}^*(\dot{\xi}_d/\Omega_s \cos \lambda) + \sin \psi_i{}^*(\dot{\eta}_d/\Omega_s \cos \lambda) \\ \\ -\sin(\psi - \psi_i{}^*) - \cos \psi_i{}^*(\dot{\eta}_d/\Omega_s \cos \lambda) + \sin \psi_i{}^*(\dot{\xi}_d/\Omega_s \cos \lambda) \end{bmatrix} \Omega_s \cos \lambda \qquad (98)$$

But

$$\psi - \psi_i{}^* = \psi - \psi_i - \Delta\psi = 0$$

Rearranging and subtracting $\Omega_s \cos \lambda$ in the first row, we have

$$\dot{\xi}_R{}^* - \Omega_s \cos \lambda = -\cos \psi_i{}^*\dot{\xi}_d + \sin \psi_i{}^*\dot{\eta}_d \qquad (99)$$

$$\dot{\eta}_R{}^* = -\sin \psi_i{}^*\dot{\xi}_d - \cos \psi_i{}^*\dot{\eta}_d \qquad (100)$$

From the last two equations the drift rates are readily determined

$$\begin{bmatrix} \dot{\xi}_d \\ \dot{\eta}_d \end{bmatrix} = - \begin{bmatrix} \cos\psi_i^* & \sin\psi_i^* \\ -\sin\psi_i^* & \cos\psi_i^* \end{bmatrix} \begin{bmatrix} \dot{\xi}_R^* - \Omega_s \cos\lambda \\ \dot{\eta}_R^* \end{bmatrix} \tag{101}$$

The procedures of gyrocompassing, equations (89) and (97), and calibration of equation (101), are indicated in figure 6.

With the drift rate biases thus established, the appropriate torquing commands $\dot{\xi}_c{}^d$ and $\dot{\eta}_c{}^d$ are applied to the LEG, as indicated in figure 6.

With the drift rates compensated, the initial gyrocompassing step, defined in equations (89) and (90), is repeated with new essentially zero drift rates $\dot{\xi}_d$ and $\dot{\eta}_d$, so that $\psi_i = \psi$ is determined with a negligible error and is applied as the initial condition ψ_o to the ψ integrator in figure 4. The computed Earth rate components $\dot{\eta}_c{}^\Omega = \Omega_s \cos\lambda \sin\psi_o$, and $\dot{\xi}_c{}^\Omega = \Omega_s \cos\lambda \cos\psi_o$ are now applied to the torquers T_η and T_ξ, respectively, as indicated in figure 6. Switches S_x and S_y, shown in figure 4, are closed simultaneously on application of $\dot{\xi}_c{}^\Omega$ and $\dot{\eta}_c{}^\Omega$. This is incorporated in the command mode shown in figure 6.

The azimuth gyro (AZG) is subjected to the Earth rate component $\Omega_s \sin\lambda$. Its output is $\dot{\psi}_m = \Omega_s \sin\lambda - \dot{\psi}_d$, where $\dot{\psi}_d$ is its drift rate. By subtracting the known quantity, $\Omega_s \sin\lambda$, $\dot{\psi}_d$ is readily determined and the appropriate compensatory torquing signal $\dot{\psi}_c{}^d$ is applied to T_ψ, as indicated in figure 6.

With the drift rates $\dot{\xi}_d$ and $\dot{\eta}_d$ eliminated by the foregoing procedure, the GIMU is also automatically calibrated, as can be verified by (61) and (62). The bias terms $g\xi_i$ and $g\eta_i$, which are due to initial offsets, are measurable. They can easily be eliminated at the GIMU output, as indicated in figure 6 by the calibration signals $g\xi_i{}^c$ and $g\eta_i{}^c$, respectively.

Summary of gyrocompassing and calibration procedure:

1. Open S_x and S_y and turn on power to LEG and AZG.

2. After warm-up time, apply $\dot{\xi}_m$ and $\dot{\eta}_m$ to ψ resolver, varying ψ_i until $\dot{\eta}_R = 0$. Store ψ_i.

3. Apply perturbation to ψ_i and determine gyrocompassing error $\Delta\psi$ by equation (97).

4. Determine $\psi_i^* = \psi_i + \Delta\psi$.

5. Apply ψ_i^* to the ψ resolver and determine $\dot{\xi}_R^*$ and $\dot{\eta}_R^*$.

6. Solve drift rates $\dot{\xi}_d$, $\dot{\eta}_d$ by equation (101).

7. Repeat gyrocompassing procedure in accordance with step 2.

8. Apply compensating torques $\dot{\xi}_c{}^d$, $\dot{\eta}_c{}^d$, $\dot{\xi}_c{}^\Omega$, $\dot{\eta}_c{}^\Omega$, and $\dot{\psi}_c{}^d$ to T_ξ, T_η, and T_ψ, respectively, simultaneously close S_x and S_y.

9. Check GIMU outputs F_{xp} and F_{yp}. If necessary, null outputs by adding $g\xi_i$ and $g\eta_i$, as indicated in figure 6.

VI. ERROR ANALYSIS AND EVALUATION

As shown in section V, errors originate primarily from angular drift rates in the LEG and AZG gyroscopes, which, for a given type of gyroscope, are essentially determined by temperature variations and g-loading. A miniature DTR gyro, described in appendix E, is chosen as the basis of the error analysis in this section.

Other errors originate in uncompensated disturbances due to friction torque, torquer scale factor errors, and gyrocompassing and alignment errors. In the analysis, x denotes position deviation, either lateral or longitudinal. In the numerical evaluation, the following constants are repeatedly used: $R = 6.378\times10^6$ m, $\omega_s = 4.46$ rad/hr, $\omega_s{}^2 = 19.93$, $180°/\pi = 57.3$.

A. Sensor Errors

1. Non-g-sensitive drift

From appendix E, the average turn-on to turn-on uncertainty is 0.03°/hr. This error is calibrated by the procedure described in section V and is compensated by the appropriate gyro torquer inputs. Assuming a compensation error of 10%, the constant residual drift rate is $d = 0.003°/\text{hr}$. From figure 8 in appendix A, for $\alpha = 0$ at 1 hr ($\zeta = 4.46$), $u = 5.4$ so that

$$\sigma_x = \frac{R\sigma_d}{\omega_s} = \frac{6.38\times10^6 \times 3\times10^{-3}}{4.46 \times 57.3} \times 5.4 = 403 \text{ m}$$

2. Temperature sensitivity

Assuming an average temperature sensitivity $S_T = 0.03°/\text{hr}/°\text{F}$ (appendix E), and the average temperature variation is a constant 0.5°F/hr, the rate of change of the drift rate is $\dot{d} = 0.015°/\text{hr}^2$. The resulting positional error obeys the same law as given in equation (D-4). At 1 hr, from figure 10, $u = 9$ and the position error is

$$\sigma_x = \frac{R\sigma_{\dot{d}}}{\omega_s{}^2}\, u = \frac{6.38\times10^6 \times 0.015}{19.93 \times 57.3} \times 9 = 754 \text{ m}$$

3. g - Sensitivity

Assuming an overall average sensitivity of $S_g = 0.05°/\text{hr/g}$, known for each individual gyroscope (appendix E), and assuming a root mean square (rms) g-input, due to turbulence, of 0.25 g, the rms drift rate is 0.0125°/hr. (Due to the low-g environment, g^2 dependence is negligible.) The bandwidth a (defined in appendix A), based on standard turbulence models (ref. 13), is in the range of 0.1 to 1.0 rad/sec. Thus, $\alpha = a/\omega_s$ is 1.5 to 15. An average $\alpha = 2$ is chosen. At 1 hr, u = 5.4 (eq. A-11)

$$\sigma_x = \frac{R\sigma_d}{\omega_s} u = \frac{6.38\times10^6 \times 0.0125}{4.46 \times 57.3} \times 5.4 = 1685 \text{ m}$$

Assuming that S_g is known to 5% or better, this error can be compensated to 1/20th of its value, by applying $F_{xp}S_{gx}^{\dot{\xi}} + F_{yp}S_{gy}^{\dot{\xi}}$ and $F_{xp}S_{gx}^{\dot{\eta}} + F_{yp}S_{gy}^{\dot{\eta}}$ to T_ξ, T_η as indicated in figure 6. Thus, the residual error is of the order of 80 m and is negligible.

A sustained acceleration (e.g., as a result of a turn, causing an $F_{yp} = 10$ m/sec^2, for a duration $\tau = 100$ sec) can be considered as an acceleration impulse, since $\omega_s\tau \ll 1$. It excites a drift rate impulse, for example, in $\dot{\eta}$

$$d = F_{yp}S_{gy}^{\dot{\eta}} = 0.05°/\text{hr/g} \times 1\text{g} = 0.05°/\text{hr}$$

This disturbance excites a position error (eqs. (82) and (83))

$$\Delta x = \frac{(gd)\tau}{\omega_s^2}(1 - \cos\omega_s\tau) = \frac{9.81\times3600^2 \times 0.05\times100}{19.93 \times 57.3 \times 3600}(1 - \cos\omega_s\tau)$$

It reaches its peak value of 150 m at $t = \pi/\omega_s = 0.704$ hr. Using the previously calculated compensation factor, this error can be reduced to ~8 m and becomes negligible.

4. Random drift in LEG gyro

Assuming an average random drift of $d = 0.005°$/hr (appendix E) and a correlation time $a^{-1} = 0.15$ hr, $\alpha = a/\omega_s = 1.5$ (appendix A). The value of u at 1 hr is, u = 3.1 (fig. 8). The resulting positional error is from equation (A-11)

$$\sigma_x = \frac{R\sigma_d}{\omega_s} u = \frac{6.38\times10^6 \times 0.05}{4.46 \times 57.3} \times 3.1 = 387 \text{ m}$$

5. Drift of AZG gyro

- <u>Error in compensating Earth rate</u>- Assuming a constant drift rate $\dot{\psi}_d = 0.1°$/hr, for moderate latitudes of ($\lambda = 45°$), $\Omega_s \cos\lambda \cong 10°$/hr, $C = \cos\psi(0.1°/\text{hr} \times 10°/\text{hr})/57.3 = \cos\psi(0.174°/\text{hr}^2)$. Then, in accordance with equation (D-4) and for u = 9 at 1 hr (fig. 10), and, e.g., $\psi = 0$,

$$\sigma_x = \frac{R\sigma_c}{\omega_s^2}\, u = \frac{6.38\times 10^6 \times 0.0174}{19.93 \times 57.3} \times 9 = 874 \text{ m}$$

It follows that the AZG can tolerate a drift rate ~10 times larger than the NEG.

Azimuth transformation error- This error is given by the first term in equation (10). Setting $\psi_A = \int \dot{\psi}_d\, dt$, the positional error, for example, in the north direction, is $\Delta x = \iint V_N \dot{\psi}_d\, dt\, dt'$. For example, if $V_N = 200$ m/sec at 1 hr,

$$\Delta x = \frac{200 \times 0.1 \times 3600^2}{3600 \times 57.3 \times 2} = 628 \text{ m}$$

6. Gyro Torquer Scale Factor Uncertainty

Torquer scale-factor uncertainty ε_T generates an equivalent drift rate of $d = (\varepsilon_T V_N)/R$. For $V_N = 200$ m/sec and $\varepsilon_T = 3\times 10^{-4}$,

$$d = \frac{3\times 10^{-4} \times 200 \times 3600 \times 57.3}{3.68\times 10^6} = 0.00336°/\text{hr}$$

From figure 8, for $\alpha = 0$, at 1 hr, $u = 5.4$. Thus,

$$\sigma_x = \frac{R\sigma_d}{\omega_s}\, u = \frac{6.38\times 10^6 \times 3.36\times 10^{-3}}{4.46 \times 57.3} \times 5.4 = 453 \text{ m}$$

The effect of scale-factor uncertainty on the AZG is readily shown to be negligible.

B. System Errors

1. Gyrocompassing Error

From equation (87) the uncorrected components of Earth rotation are given by

$$\Delta\dot{\xi} = \Delta\psi \sin\psi_o \quad \Omega_s \cos\lambda$$

$$\Delta\dot{\eta} = \Delta\psi \cos\psi_o \quad \Omega_s \cos\lambda$$

Assuming a gyrocompassing error (sec. V) of $\Delta\psi = 0.05°$, the rate errors, $\Delta\dot{\xi}$ and $\Delta\dot{\eta}$, at moderate latitudes of $\Omega_s \cos\lambda = 10°/\text{hr}$, are of the order of $10°/\text{hr} \times 0.05°/57.3 = 0.0087°/\text{hr}$. This is equivalent to a constant drift rate d for which $\alpha = 0$ in figure 8. At 1 hr, $u = 5.4$, and the positional error is by equation (A-11)

$$\sigma_x = \frac{R\sigma_d}{\omega_s} u = \frac{6.38\times10^6 \times 0.0087 \times 5.4}{4.46 \times 57.3} = 1172 \text{ m}$$

2. Reaction Torque of the AZG

The AZG, being subjected to heading rate input $\dot{\psi}$, exerts a torque $H\dot{\psi}$. If its spin axis is along X_ℓ, this torque is around Y_ℓ. For $H = 8$ g cmsec and typical values for $\dot{\psi}$ of 0.1 rad/sec, this torque amounts to $M_\psi = 8 \times 0.1 = 0.8$ g cm. Since the pendulosity $W\ell$ of the GIMU is assumed to be 200 g cm, this precession torque is equivalent to an acceleration angle

$$\varepsilon = \dot{\psi}H/(W\ell) = 0.8/200 = 0.004 \text{ rad}$$

or, an acceleration error of $\varepsilon g = 0.04$ m/sec^2. Assuming that H is known to 1% accuracy, this disturbance can be computed, scaled, and subtracted from the GIMU output as indicated in figure 6. With these assumptions, the residual acceleration disturbance is $\varepsilon_r = 40$ µrad. If, $\dot{\psi}$, in a turn persists, for example, for $\tau = 100$ sec, then, since $\omega_s\tau << 1$, this can be considered as a velocity impulse exciting a position error (see eqs. (82) and (83)),

$$\Delta x = \frac{g\varepsilon_r\tau}{\omega_s} \sin \omega_s t \; .$$

It reaches its peak of

$$\Delta x = \frac{9.81 \times 40\times10^{-6} \times 100 \times 3600}{4.46} = 31.6 \text{ m}$$

at $t = \pi/2\omega_s = 0.352$ hr. This is a negligible error.

Assuming that the rms value of $\dot{\psi}$ (due to turbulence) is 0.1 rad/sec, at an average angular frequency of $a = 0.5$ rad/sec, the average value of $\alpha = a/\omega_s$ is 6.7. The corresponding u in figure 9 at 1 hr is $u = 0.9$. In accordance with equation (C-2), the positional error at 1 hr is:

$$\sigma_x = R\sigma_{\varepsilon r}u = 6.38\times10^6 \times 40\times10^{-6} \times 0.9 = 230 \text{ m}$$

With the above compensation of 1%, this error is negligible.

3. Initial Tilt Error

From equations (82) and (83), the effect of an initial tilt error η_i, ξ_i denoted here by ε_i results in a positional error,

$$\Delta x = g\varepsilon_i(1 - \cos \omega_s t)/\omega_s{}^2$$

Assuming that $\varepsilon_i = 100$ µrad, Δx at 1 hr is

$$\Delta x = \frac{9.81 \times 3600^2 \times 100 \times 10^{-6}}{19.93} (1 - \cos 4.46) = 797 \text{ m}$$

4. Bearing Friction Torque Disturbance

Gimbal bearing friction is modeled as dry friction exerting a constant torque, T_f, due to the pitch and roll motion of the airframe, with respect to the gimbal axis frame. The significance of this assumption is that the torque signals can be modeled as a random binary process fluctuating between $+T_f$ and $-T_f$, with a zero crossing rate a, determined by the frequency of the random pitch and roll motion excited by turbulence. It is known (ref. 14) that the autocorrelation function of such a binary process is

$$\phi_{ff}(\tau) = T_f^2 \, e^{-2a|\tau|}$$

The acceleration error induced by this torque noise is $\varepsilon = T_f/W\ell$, so that

$$\phi_{\varepsilon\varepsilon}(\tau) = \sigma_\varepsilon^2 \, e^{-2a|\tau|}$$

Typical values of T_f are 0.05 g cm; and since $W\ell$ is assumed to be $W\ell = 200$ g cm, $\sigma_\varepsilon = 0.05/200 = 250$ µrad.

Assuming again, $a = 0.5 \text{ sec}^{-1}$, the value of α is $\alpha = 2a/\omega_s = 13.4$. In accordance with figure 9, the value of u at 1 hr is $u = 0.5$, and the positional error in accordance with equation (C-2) is:

$$\sigma_x = R\sigma_\varepsilon u = 6.38 \times 10^6 \times 250 \times 10^{-6} \times 0.5 = 796 \text{ m}$$

Since the friction model is known, an estimate of ε can be provided in real time, and a large portion of the friction noise $g\varepsilon$ can be cancelled by subtraction.

5. Dead Band Due to Bearing Friction

By the same numerical assumptions as in equation (B-4), the bearing friction causes a dead band of 250 µg in the acceleration measurement corresponding to 250 µrad. It can be effectively linearized by injecting dither signals to the LEG torquers T_ξ and T_η. Assuming a sinusoidal dither signal of a frequency $f_d = 5$ Hz (see sec. V) to provide an angular amplitude of ~10 times the dead band, that is, $\alpha_d = 2.5$ mrad, the peak torquing rate r_T is

$$r_T = \alpha_d \omega_d = 2.5 \times 10^{-3} \times 2\pi f_d \times 57.3 = 4.5°/\text{sec} .$$

In accordance with appendix E, this is well within the torquer capacity of the gyros considered. In accordance with reference 15, the system is essentially linearized.

6. Gimbal Torquer Scale-Factor Error

Error in Schuler tuning- A scale-factor error b_x, b_y in the gimbal torquers is mathematically equivalent to the gyro torquer scale-factor errors discussed in section VI. In accordance with reference 9 it is assumed that the errors in b_x, b_y, denoted ε_b are $\sim 10^{-4}$. In accordance with section VI this would produce an equivalent drift rate of less than 0.001°/hr, and a positional error (at 1 hr) of 133 m, which is negligible.

Proportionality error- The position error is directly proportional to $\varepsilon_b = 10^{-4}$. For $V_N = 200$ m/sec, at 1 hr, the error is

$$\Delta x = 10^{-4} \times 200 \times 3600 = 72 \text{ m}$$

which is also a negligible error.

Summary

The principal contributing factors to positional error at 1 hr of flight are summarized in table II. They are treated as statistically independent, and the total error is the resultant rms value. The total rms positional error after 1 hr of flight is 2210 m or 1.2 n. mi.

The individual rms error propagation time histories listed in table II are shown in figure 11 up to 2 hr, along with the total rms error denoted by σ_x^T. It is typical that from these results the initial large tilt error of 100 μrad, assumed in section VI-3, causes a relatively rapid positional divergence in the first 0.5 hr, whereas the constant drift rate of temperature, assumed in section VI-2 causes a relatively rapid divergence after ~50 min. An alternative model is to assume a smaller initial tilt error of 25 μrad, and a stationary random temperature variation of 1° F and a correlation time of $a^{-1} = 1$ min, for which $\alpha = a/\omega_s = 60/4.46 = 14$. The results are shown in figure 12. The short-term divergence is considerably reduced, but no significant change is incurred around 1 hr of flight. In a third error model, the AZG has a drift rate of 0.05°/hr instead of 0.1°/hr; the initial tilt error is as in the first model, and the temperature model is as in the second. The results are shown in figure 13.

It is significant that with all three models the positional divergence at 1 hr clusters around 2 km. The third model evidently has a smaller divergence beyond 1 hr.

VII. CONCLUSIONS

It has been shown that the low-g environment assumed in this report permits a significant simplification in mechanization by dispensing with the accelerometers, since moderate size gimbal torquers can provide the required torques for specific force measurements. This device constitutes a two-axis locally level accelerometer, which is easily integrated with an on-board microcomputer to constitute a complete inertial measurement unit. Rapid gyrocompassing is achieved by virtue of the large pendulosity of the gimbal system and by strapdown type resolving of the LEG outputs.

Gyro drift rates are determined as part of the gyrocompassing process. Since the essential inertial measurements are derived from one sensor (LEG), complex instrument alignment is circumvented. Bias errors due to possible correlated gyro and accelerometer noise components are not present. The gyros, in particular the LEG, being essentially isolated from airframe motion, require only minute torquer activity, so that temperature fluctuations are also small. In addition, the low-g environment renders the g and g^2 sensitive errors sufficiently small so that gyros of moderate cost can be used.

Modern miniature DTR gyroscopes are sufficiently small so that both the LEG and AZG can be mounted within the inner gimbal g_i. Thus, the complete assembly is expected to be comparable in size and weight to a conventional vertical gyroscope. The error analysis, based on state-of-the-art sensor data, demonstrates that a navigation error of the order of 1 n. mi. at 1 hr of flight can be achieved.

APPENDIX A

POSITIONAL ERROR PROPAGATION DUE TO RANDOM GYRO DRIFT RATE

The specific force measurement error in a Schuler tuned system is given in equations (82) and (83). ξ_E° and η_N°, which are angular deviations from the local vertical, consist of constant, random stationary, and divergent terms, as indicated in equations (69) and (70). In this appendix, the following uniform notation is used for the drift rates $\dot{\xi}_d$ or $\dot{\eta}_d$ contributing to ξ_E° and η_N°:

d - gyro angular drift rate, defined in geographical coordinates (rad/hr).

ω_s - Schuler frequency (rad/hr).

R - distance of vehicle from the center of the Earth (meters).

a^{-1} - correlation time of gyro drift rate process (hours).

$\alpha \triangleq a/\omega_s$.

$\zeta \triangleq \omega_s t$.

The drift rate is modeled as a first-order Markov process with the autocorrelation function

$$\phi_{dd}(\tau) = \sigma_d^{\,2}\, e^{-a|\tau|} \tag{A-1}$$

where $\sigma_d{}^2 = V_{ar}(d)$. The corresponding power density spectrum of d is

$$\Phi_{dd}(s) = \sigma_d^{\,2} \frac{2a}{a^2 - S^2} \tag{A-2}$$

The spectrum of positional deviation x as derived from equations (82) and (83) is

$$\Phi_{xx}(S) = \sigma_d^{\,2} g^2 \frac{2a}{-S^2(a^2 - S^2)(\omega_s^{\,2} + S^2)(\omega_s^{\,2} - S^2)} \tag{A-3}$$

In time domain, $V_{ar}(x) = \sigma_x{}^2$ is given by

$$\sigma_x^{\,2} = \int_o^t \int_o^t h_x(\tau')h_x(\tau'')\phi_{dd}(\tau' - \tau'')d\tau'\, d\tau'' \tag{A-4}$$

where the impulse response $h_x(t)$, corresponding to $H_x(S) = 1/S(S^2 + \omega_s{}^2)$ in equation (A-3), is

$$h_x(t) = \frac{1}{\omega_s^2}(1 - \cos \omega_s t) \tag{A-5}$$

Substituting equations (A-1) and (A-5) in (A-4) and normalizing by $\sigma_d^2 g^2$, the double convolution integral is

$$\begin{aligned} I &= \frac{1}{\omega_s^4}\int_o^t \int_o^t (1 - \cos \omega_s\tau')(1 - \cos \omega_s\tau'')e^{-a|\tau'-\tau''|}\, d\tau'\, d\tau'' \\ &= \frac{1}{\omega_s^6}\int_o^\zeta \int_o^\zeta (1 - \cos \nu')(1 - \cos \nu'')e^{-\alpha|\nu'-\nu''|}\, d\nu'\, d\nu'' \end{aligned} \tag{A-6}$$

By the change of variables $\lambda = \nu' - \nu''$, equation (A-6) is transformed to

$$\begin{aligned} I &= \frac{1}{\omega_s^6}\int_{\nu'=0}^{\zeta} (1 - \cos \nu')\int_{\nu'}^{\nu'\zeta} [1 - \cos(\nu' - \lambda)]e^{-\alpha|\lambda|}(-d\lambda)d\nu' \\ &= \frac{1}{\omega_s^6}\int_{\nu'=0}^{\zeta} (1 - \cos \nu')\left\{\int_{\nu'-\zeta}^{o} [1 - \cos(\nu' - \lambda)]e^{\alpha\lambda}\, d\lambda \right. \\ &\quad \left. + \int_o^{\nu'} [1 - \cos(\nu' - \lambda)]e^{-\alpha\lambda}\, d\lambda\right\}d\nu' \end{aligned} \tag{A-7}$$

The result of the integration of equation (A-7) is

$$\begin{aligned} I = \frac{1}{\alpha^2(\alpha^2+1)^2}&\left\{\alpha\zeta(3\alpha^2+2)(\alpha^2+1) + 2(1-e^{-\alpha\zeta})(\alpha^2+1)[\alpha(\alpha \cos \zeta - \sin \zeta) - 1]\right. \\ &+ 2\alpha^3 e^{-\alpha\zeta}(\alpha \cos \zeta - \sin \zeta) - \alpha^3(\alpha^2 + 1)\, 4\left(\sin \zeta - \frac{\sin 2\zeta}{4}\right) \\ &\left. - \alpha^2\left(\alpha^2 + \alpha^2 \cos^2 \zeta - \sin^2 \zeta\right)\right\} \end{aligned} \tag{A-8}$$

For

$$\alpha \to 0 , \qquad I = (\zeta - \sin \zeta)^2 \tag{A-9}$$

For

$$\alpha \to \infty , \qquad I = \frac{1}{\alpha}\left(3\zeta - 4 \sin \zeta + \frac{\sin 2\zeta}{2}\right) \tag{A-10}$$

Defining $u \triangleq (I)^{1/2}$, the standard deviation of x, σ_x is

$$\sigma_x = \frac{R\sigma_d}{\omega_s} u \qquad \text{(A-11)}$$

Plots of $u(\alpha, \xi)$ are shown in figure 8.

APPENDIX B

VELOCITY ERROR PROPAGATION DUE TO RANDOM GYRO DRIFT RATE

Using the same notations and definitions as in appendix A, the spectrum of the velocity error v is given by

$$\Phi_{vv}(S) = \sigma_d^2 g^2 \frac{2a}{(a^2 - S^2)(\omega_s^2 + S^2)(\omega_s^2 - S^2)} \tag{B-1}$$

In time domain, $V_{ar}(v) = \sigma_v^2$ is given by

$$\sigma_v^2 = \int_o^t \int_o^t h_v(\tau')h_v(\tau'')\phi_{dd}(\tau' - \tau'')d\tau' \, d\tau'' \tag{B-2}$$

where $h_v(t)$, corresponding to $H_v(S) = 1/(\omega_s^2 + S^2)$ is

$$h_v(t) = \frac{1}{\omega_s} \sin \omega_s t \tag{B-3}$$

Substituting equations (B-1) and (B-3) into equation (B-2) and normalizing by $\sigma_d^2 g^2$, the double convolution integral is

$$I = \frac{1}{\omega_s^2} \int_o^t \int_o^t \sin \omega_s\tau' \sin \omega_s\tau'' \, e^{-a|\tau'-\tau''|} \, d\tau' \, d\tau''$$

$$= \frac{1}{\omega_s^2} \int_o^\zeta \int_o^\zeta \sin \nu' \sin \nu'' \, e^{-\alpha|\nu'-\nu''|} \, d\nu' \, d\nu'' \tag{B-4}$$

By changing variables $\lambda = \nu' - \nu''$, equation (B-4) is transformed to

$$I = \frac{1}{\omega_s^4} \int_{\nu'=0}^{\zeta} \sin \nu' \left\{ \int_{\nu'-\zeta}^{\nu'} \sin(\nu' - \lambda)e^{-\alpha|\lambda|} \, d\lambda \right\} d\nu'$$

$$= \frac{1}{\omega_s^4} \int_{\nu'=0}^{\zeta} \sin \nu' \left\{ \int_{\nu'-\zeta}^{o} \sin(\nu' - \lambda)e^{\alpha\lambda} \, d\lambda + \int_o^{\nu'} \sin(\nu' - \lambda)e^{-\alpha\lambda} \, d\lambda \right\} d\nu' \tag{B-5}$$

The result of the integration of equation (B-5) is

$$I = \frac{1}{(\alpha^2 + 1)^2} \left\{ \alpha(\alpha^2 + 1)\left(\zeta - \frac{\sin 2\zeta}{2}\right) - (\alpha^2 \sin^2 \zeta - \cos^2 \zeta) \right.$$

$$\left. - 2(\alpha \sin \zeta + \cos \zeta)e^{-\alpha\zeta} + 1 \right\} \tag{B-6}$$

For

$$\alpha \rightarrow 0 , \qquad I = (1 - \cos \zeta)^2 \tag{B-7}$$

For

$$\alpha \rightarrow \infty , \qquad I = \frac{1}{\alpha}\left(\zeta - \frac{\sin 2\zeta}{2}\right) \tag{B-8}$$

Defining $u \triangleq (I)^{1/2}$, the standard deviation of v, σ_v is

$$\sigma_v = R\sigma_d u \tag{B-9}$$

Plots of $u(\zeta, \alpha)$ are shown in Figure 9.

APPENDIX C

POSITIONAL ERROR PROPAGATION DUE TO RANDOM ACCELERATION ERROR

Using the same notations and definitions as in appendixes A and B and by denoting the acceleration error as $g\varepsilon$ (where ε is an equivalent tilt angle from the local vertical), then the spectrum of the positional deviation x is

$$\Phi_{xx}(S) = \sigma_\varepsilon{}^2 g^2 \frac{2a}{(a^2 - S^2)(\omega_s{}^2 + S^2)(\omega_s{}^2 - S^2)} \tag{C-1}$$

where

$$\sigma_\varepsilon{}^2 = \mathrm{var}(\varepsilon)$$

This has the same structure as equation (B-1) and therefore results in the same I as given in equation (B-6). Consequently, the standard deviation of x, σ_x is

$$\sigma_x = R\sigma_\varepsilon u \tag{C-2}$$

A plot of $u(\zeta, \alpha)$ is shown in figure 9.

APPENDIX D

POSITIONAL ERROR PROPAGATION DUE TO CONSTANT HEADING DRIFT RATE ERROR

From equation (86), the uncertainty in determining the Earth rate compensating precession command is $\Delta\dot{\eta} = \Delta\psi\Omega_s \cos \lambda$. Assuming perfect gyrocompassing, that is, a precise initial value for ψ_o, and a constant unknown azimuth gyro drift rate $\dot{\psi}_d$ then $\Delta\psi = \dot{\psi}_d t$, so that the equivalent drift rate due to this compensation error is

$$C = \dot{\psi}_d \Omega_s \cos \lambda \tag{D-1}$$

The positional divergence σ_x due to this error in accordance with equations (82) and (83) is

$$\sigma_x = g\sigma_c \frac{1}{S^3(\omega_s^2 + S^2)}$$

In time domain

$$\sigma_x = g\sigma_c \left[\frac{1}{\omega_s^4} (\cos \omega_s t - 1) + \frac{1}{2\omega_s^2} t^2\right] \tag{D-2}$$

Defining

$$u \triangleq \frac{\zeta^2}{2} - (1 - \cos \zeta) \tag{D-3}$$

σ_x is given by

$$\sigma_x = \frac{R\sigma_c}{\omega_s^2} u \tag{D-4}$$

A plot of $u(\zeta)$ is shown in figure 10.

APPENDIX E

TYPICAL PERFORMANCE CHARACTERISTICS OF A DRY-TUNED ROTOR GYROSCOPE

1. Physical data

- Size	1 in. diam × 1 in. length
- Weight	80 g
- Angular momentum	8 g cmsec
- Maximum rate input	100°/sec
- Temperature control	Integral; sensor + heater

2. Average drift rate characteristics

- Repeatability (turn-on to turn-on — non-g-sensitive)	0.025°/hr 1σ
- g-sensitive drift (including quadrature)	0.02°/hr 1σ
- Anisoelasticity	$0.02°/hr/g^2$ 1σ
- Torquer scale-factor stability	50÷200 ppm
- Temperature sensitive drift	0.03°/hr/°F 1σ
- Torquer scale-factor temperature sensitivity	0.035°/。/°F 1σ
- Random drift rate with correlation time of 0.15 hr	0.005°/hr 1σ

3. Environment operating range

- Temperature	-40°F to 160°F
- g-capability	better than 200 g
- Maximum transient rate input	300°/sec

REFERENCES

1. Garg, S. C.; Morrow, L. D.; and Mamen, R.: Strapdown Navigation Technology: A Literature Survey. AIAA J. of Guidance and Control, vol. 1, no. 3, May-June 1978, pp. 161-172.

2. Peterson R.: Advantages of Gimballed Inertial Navigation Systems. NAECON 1976 Record, pp. 508-513.

3. Farrell, J. L.: Integrated Aircraft Navigation, Academic Press, 1976, pp. 104-105.

4. Bar Itzhack, I. Y.: Optimal Updating of INS Using Sighting Devices, AIAA J. of Guidance and Control, vol. 1, no. 5, Sept.-Oct. 1978, pp. 305-312.

5. Bryson, A. E.: Kalman Filter Divergence and Aircraft Motion Estimators, AIAA J. of Guidance and Control, vol. 1, no. 1, Jan-Feb. 1978, pp. 71-79.

6. Monaco, S. J., and Audly, D. R.: Schuler Tuned Vertical Indicating System, AIAA J. of Guidance and Control, vol. 1, no. 6, Nov.-Dec. 1978, pp. 413-419.

7. Hector, F.: The Ramp Inertial Navigation System, Philips Technical Review, vol. 29, no. 3-4, 1968, pp. 69-85.

8. Astrom, K. J.; and Hector, N. F.: Vertical Indication with a Physical Pendulum Based on Electromechanical Synthesis of a High Moment of Inertia, Report No. 590802 - TTN Group, Division of Applied Hydromechanics, Royal Institute of Technology, Stockholm, Sweden, Aug. 1959.

9. Koenke, E. J.: Analysis and Evaluation of a Novel Inertial Navigation System, NASA TN D-5456, Nov. 1969.

10. Craig, Robert J. G.: Theory of Operation of an Elastically Supported Tuned Gyroscope, IEEE Trans. on Aerospace and Electronic Systems, vol. AES-8, no. 3, May 1972, pp. 280-288.

11. Ronald, N. A.; and Maunder, L.: Gyrodynamics and its Engineering Applications. Academic Press, 1961, Chap. 12.

12. Kayton, M.; and Fried, W. R.: Avionics Navigation Systems, Wiley, 1969, Chapt. 7, p. 323.

13. Heffley, R. K.: A Study of Key Features of Random Atmospheric Disturbance Models for the Approach Flight Phase, AIAA Atmospheric Flight Mechanics Conference, Aug. 1977.

14. Melsa, J. L.; and Sage, A. P.: An Introduction to Probability and Stochastic Processes, Prentice-Hall, 1973, Chap. 5.

15. Gelb, A.; Van der Velde, W. E.: Multi-Input Describing Functions and Non-Linear Systems Design, McGraw-Hill, 1968.

TABLE I.- SYSTEM CONSIDERATIONS IN GIMBALLED AND STRAPDOWN MECHANIZATIONS SUBJECT TO ASSUMPTIONS 1 THROUGH 9

Category	Mechanization	
	Gimballed	Strapdown
Specific force sensors	At least[a] two in the 10^4 dynamic range class	At least[a] three in the 10^4 dynamic range class
Gyroscopes - dry tuned rotor (DTR) - TDF type[b]	At least two[a]: One in the 0.1°/hr class and one in the 0.01°/hr class. Dynamic range: 10^3.	At least[a] two: Both in the 0.01°/hr class. Dynamic range: 40×10^6.
Attainability of 0.01°/hr gyro performance	Moderate cost due to low gyro torquer activity.	High cost due to high gyro torquer activity.
Mechanical assembly	At least three gimbals with three torquer - pickoff pairs.	Fixed mounting. (Three dithering torquers for laser gyros.)
Electronic circuitry	Sensor interfaces, platform servos, temperature controllers.	Sensor interfaces, temperature controllers, (control circuitry for laser gyros).
Computational load	Integration of navigation equation, compensating torques for Earth rotation.	Integration of naviagtion equation, compensating torques for earth rotation, direction cosine matrix, transformation to geographical coordinates.
Susceptibility to vibration and shock	Low, due to rotational isolation by platform.	Potentially high, due to possible correlated noise in gyros and specific force sensors.
Alignment and bias calibration	Insensitive to airframe orientation. One calibration valid for arbitrary flight profile. No special devices required.	Sensitive to airplane orientation. Many calibration points are required for arbitrary flight profile. Special calibrating device required.
Availability of attitude rate information	By differentiation of gimbal pickoff readings.	Directly available from the body mounted gyros.

[a]"At least" refers to possible redundancy requirements.
[b]This type is currently a valid comparison with strapdown mechanizations.

TABLE II.- RMS POSITIONAL ERRORS AFTER 1 HR

Section		Description of error source	rms error at 1 hr, m
1	VI-A1	Non-g-sensitive gyro drift	403
2	VI-A2	Drift rate, due to temperature variation	754
3	VI-A4-a	Drift rate, due to error in Earth rate compensation	874
4	VI-A4-b	Distance-related error due to AZG drift	628
5	VI-A5	Random drift rate in LEG	387
6	VI-A6	Gyro torquer scale-factor uncertainty	453
7	VI-B1	Gyrocompassing error	1172
8	VI-B3	Initial tilt error	797
9	VI-B4	Gimbal bearing friction torque	796
		Total rms error	2210

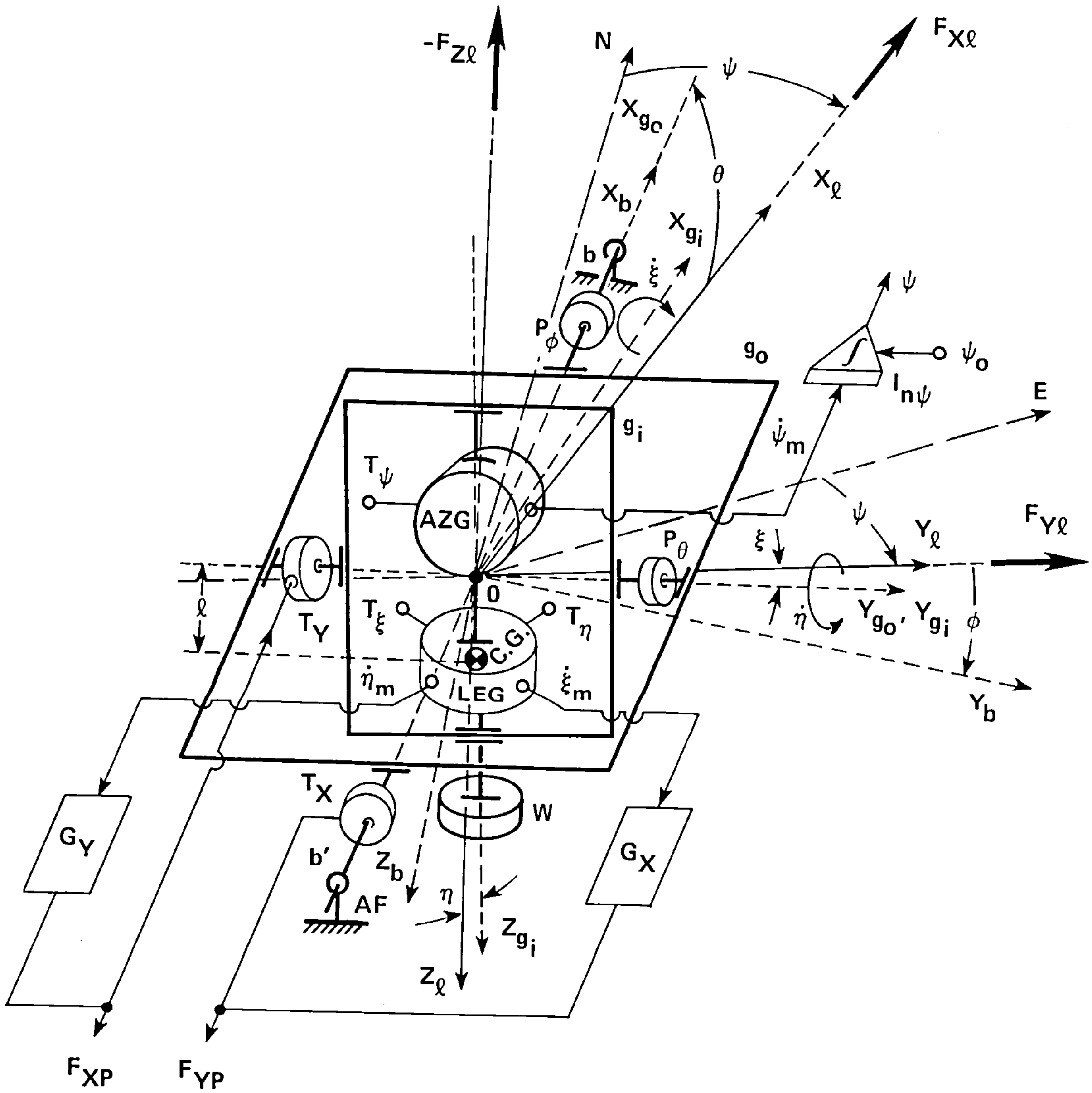

Figure 1.- Description and definition of the axis system of the two-gimbal gyro pendulum and principal loop closures.

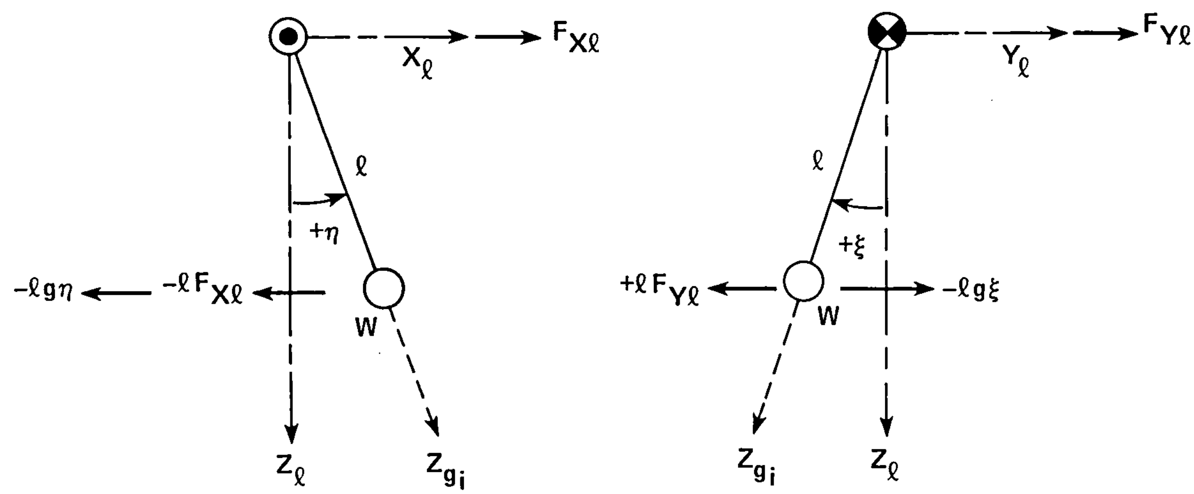

Figure 2.- Sign notations of forces and torques in the locally level plane.

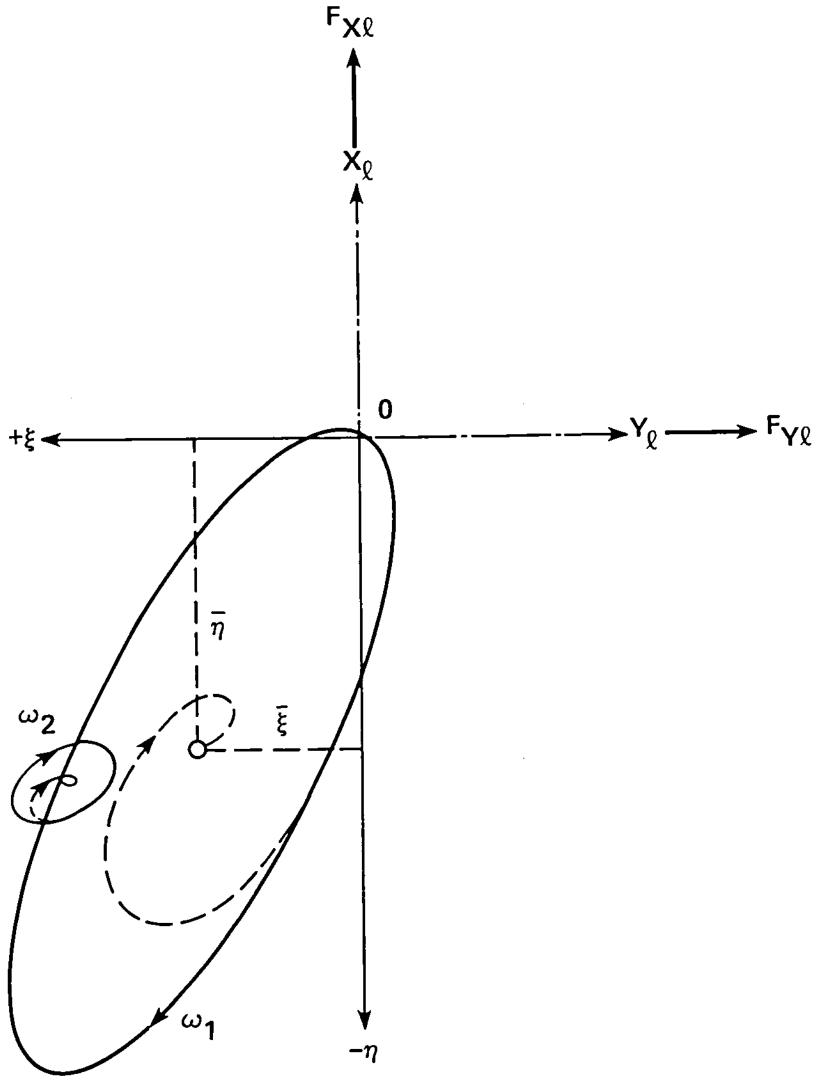

Figure 3.- Trajectory of the gyro-pendulum motion in the ξ,η plane in response to $F_{y\ell}$ and $F_{x\ell}$.

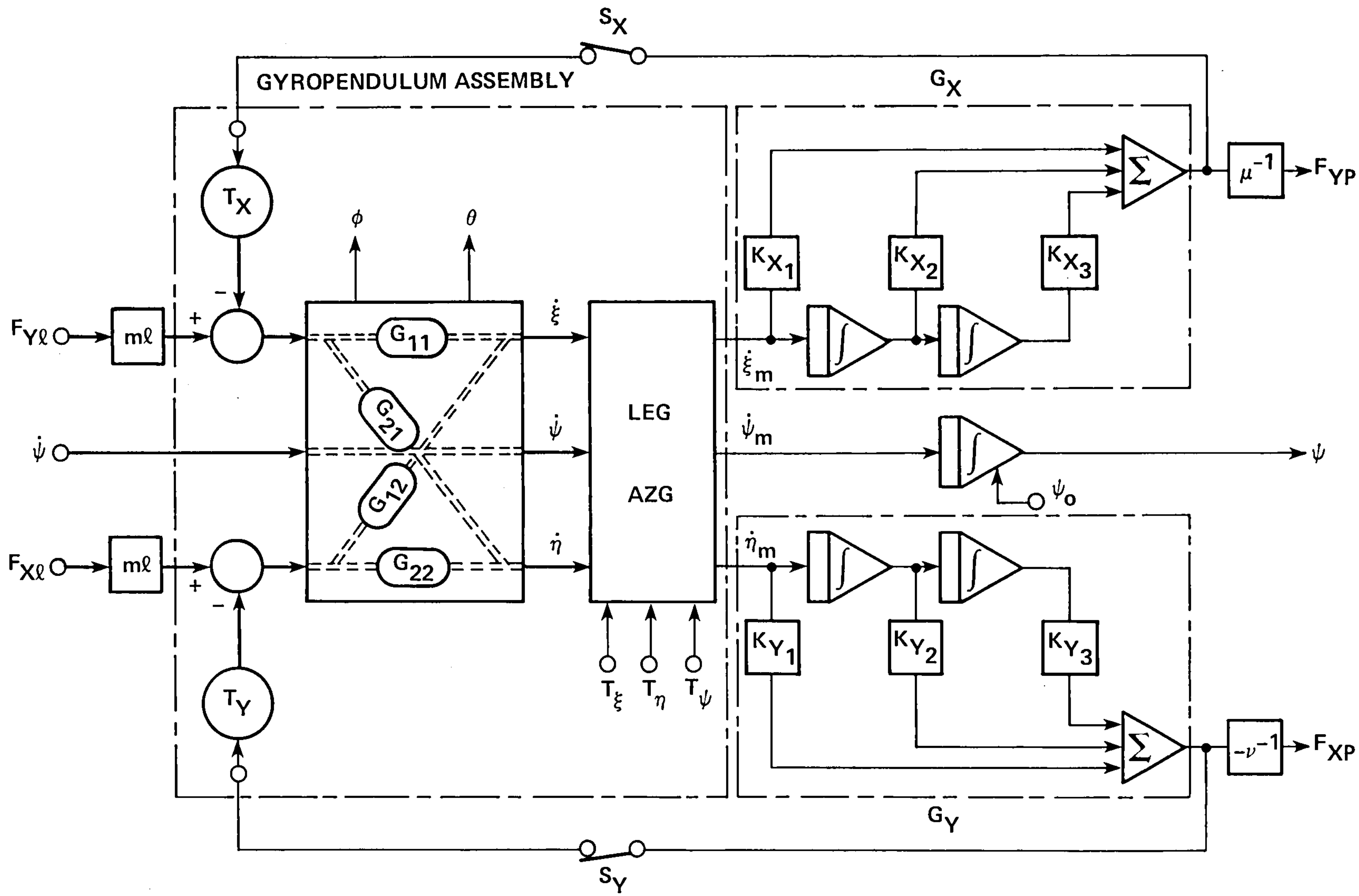

Figure 4.- Block diagram of the GIMU and implementation of its control loops.

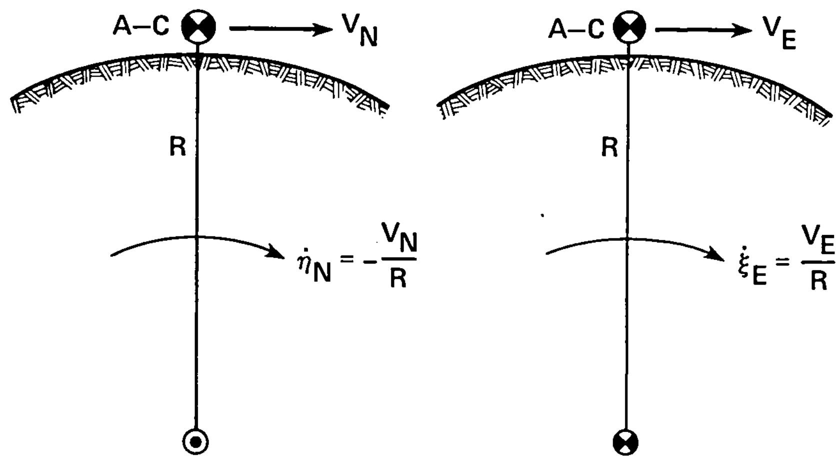

(a) Sign conventions for $\dot{\eta}_N$ and $\dot{\xi}_E$.

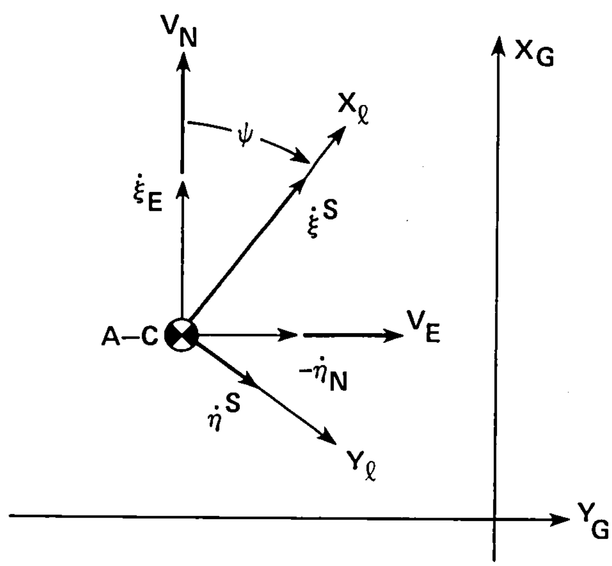

(b) Schuler torquing rates in body axes.

Figure 5.- Definition of angular rates in geographical and body axis systems.

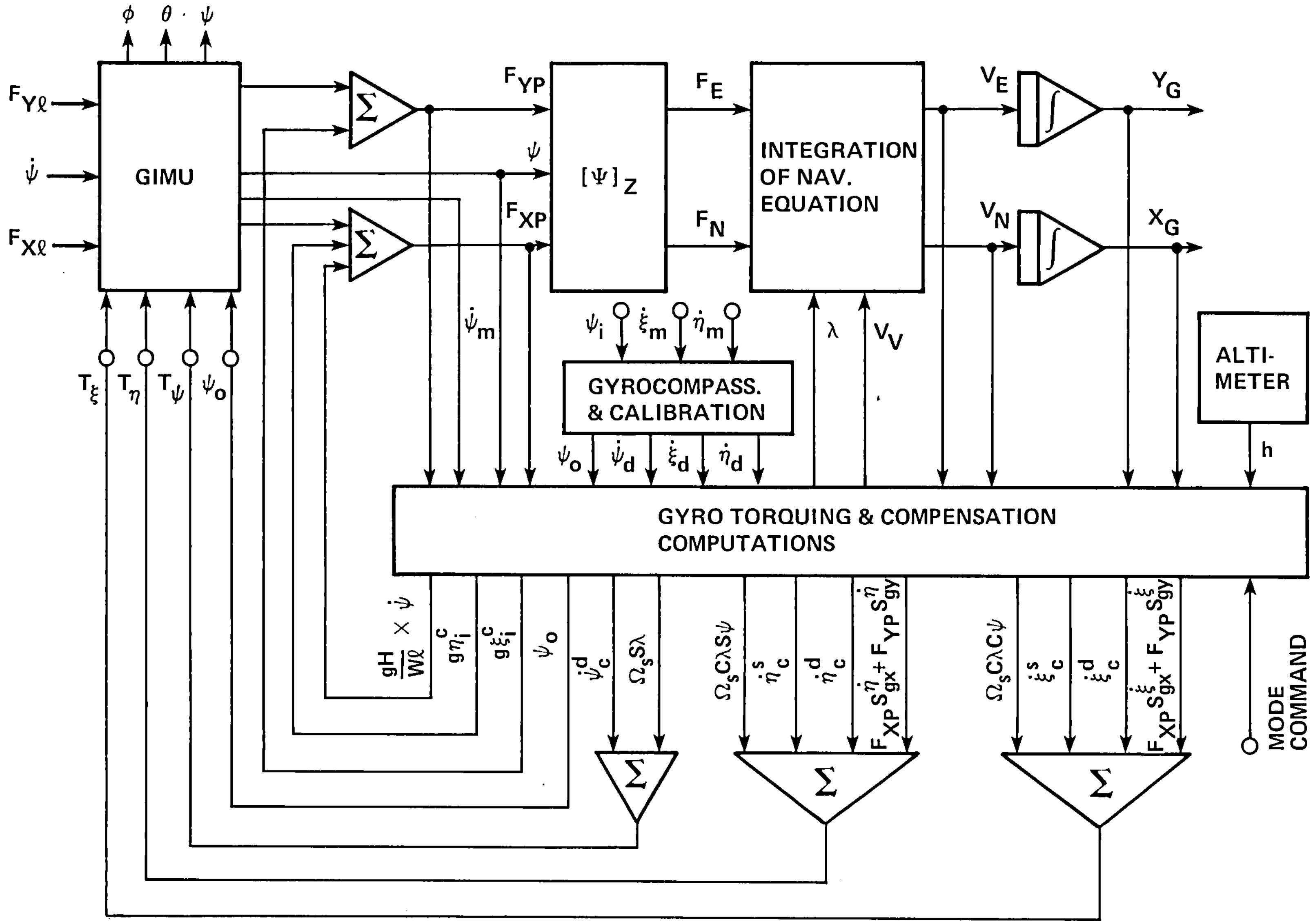

Figure 6.- Integration of the GIMU in a complete inertial measurement system.

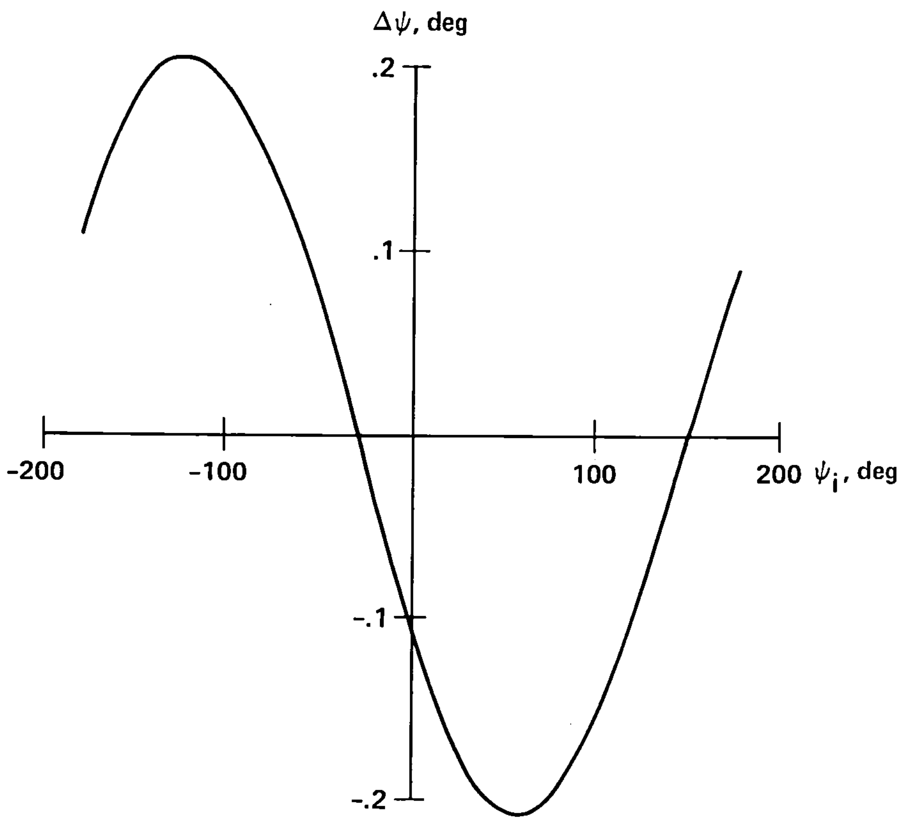

Figure 7.- Example of gyrocompassing error $\Delta\psi$ as a function of ψ_i for gyro-drift rates $\dot{\xi}_d = 0.03°/hr$ and $\dot{\eta}_d = 0.02°/hr$.

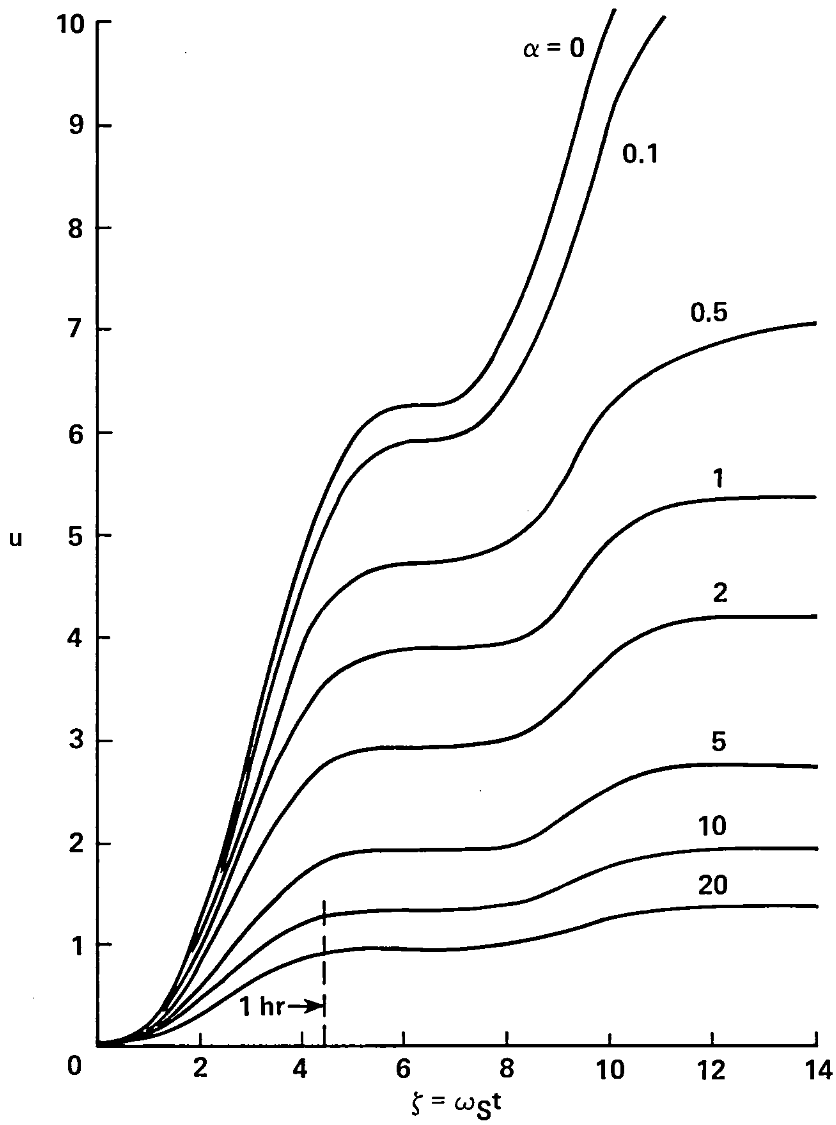

Figure 8.- Normalized positional error propagation as a function of normalized time $\zeta = \omega_s t$ with gyro noise bandwidth $a = \alpha\omega_s$ as a parameter.

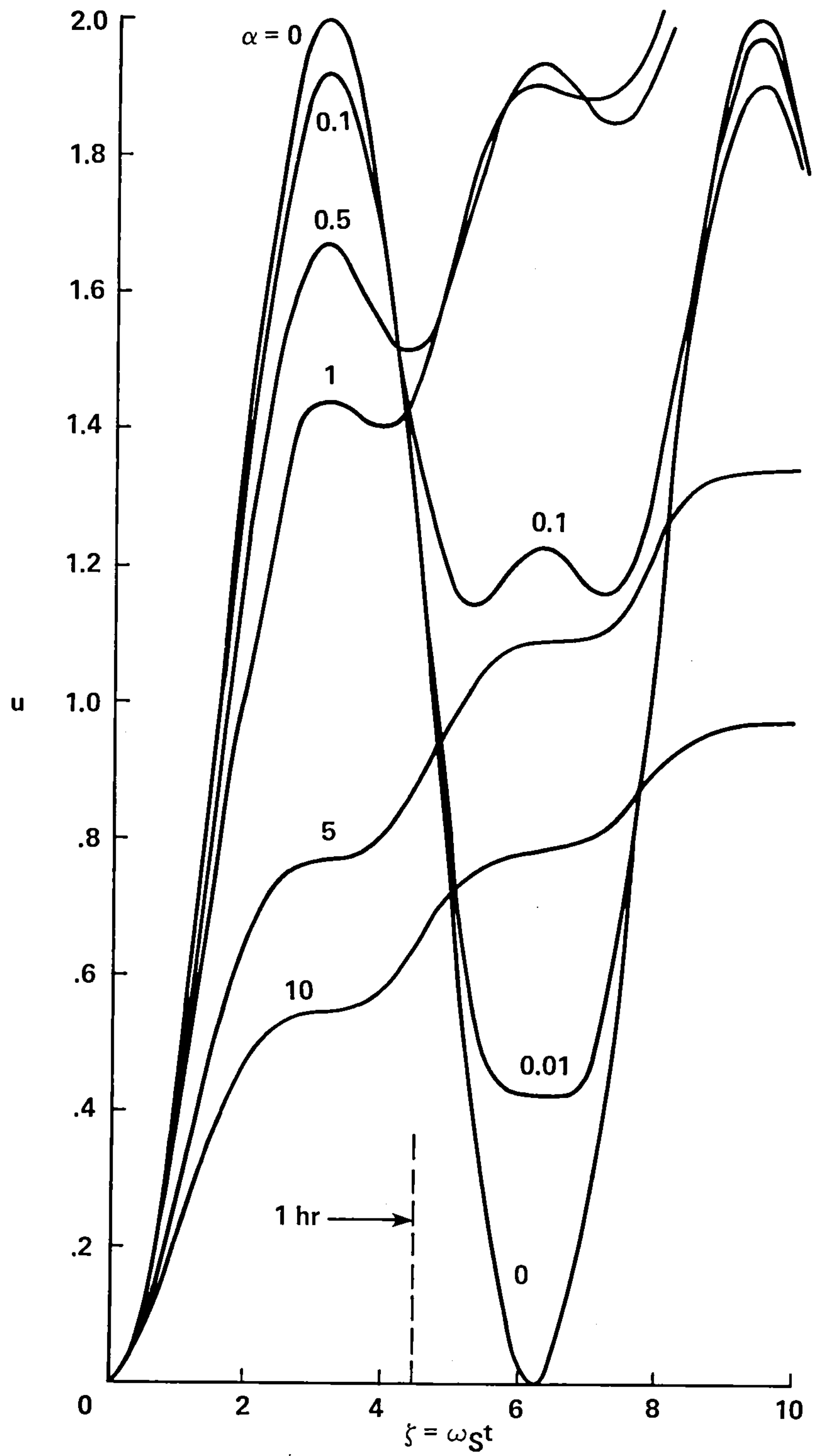

Figure 9.- Normalized velocity error propagation as a function of normalized time $\zeta = \omega_s t$ with gyro noise bandwidth $a = \alpha\omega_s$ as a parameter, or normalized position error with accelerometer noise bandwidth $a = \alpha\omega_s$ with a as a parameter.

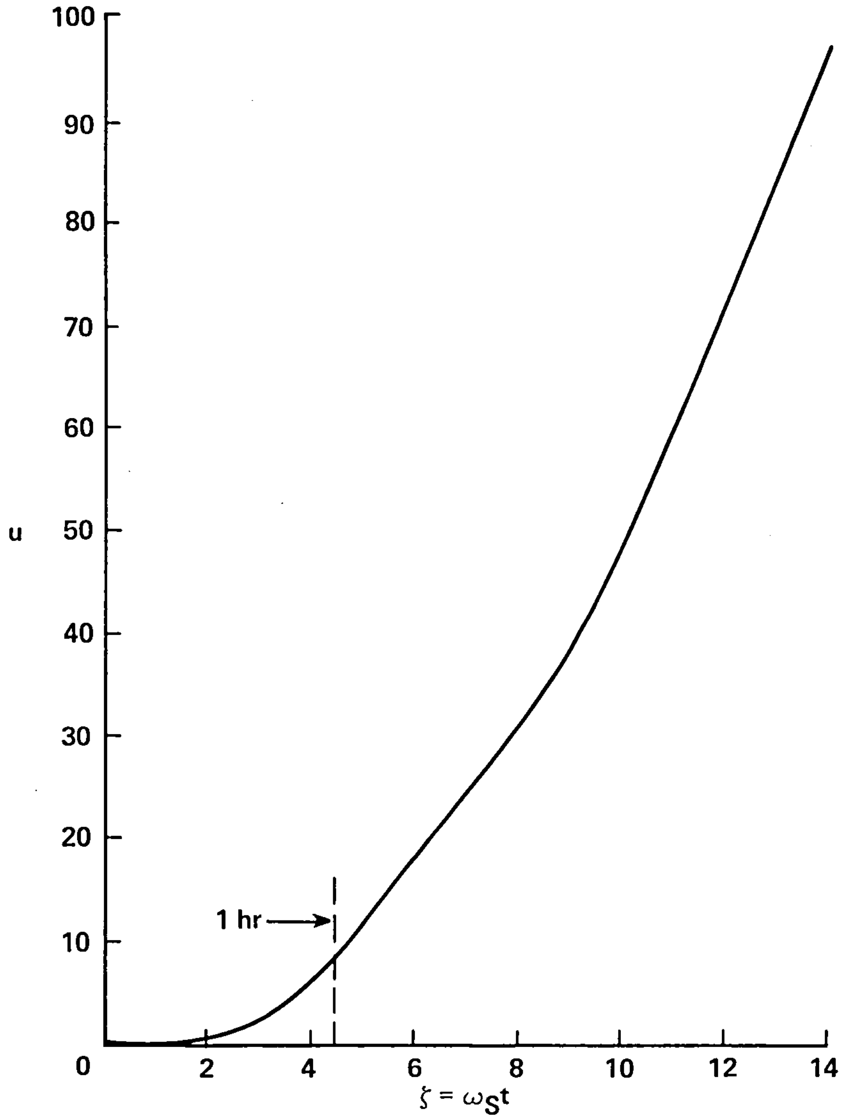

Figure 10.- Normalized error propagation as a function of normalized time $\zeta = \omega_s t$ for a constant AZG drift rate $\dot{\psi}_d$ or a constant rate of change of temperature of the LEG.

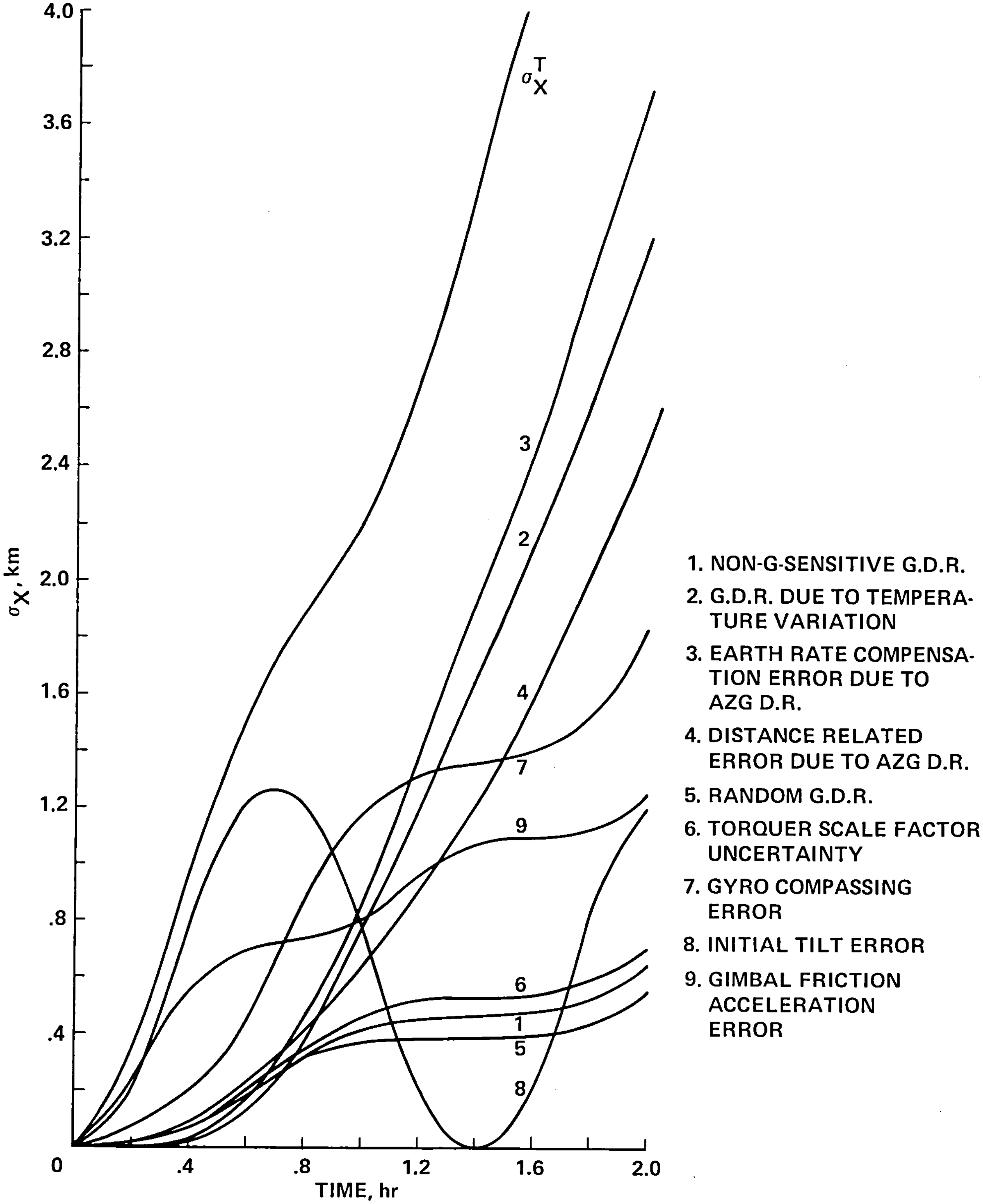

Figure 11.- Positional error propagation with a 100 μrad initial tilt error, constant drift rate of the AZG of $\dot{\psi}_d$ = 0.1°/hr, and a constant temperature slope of the LEG of 0.5° F/hr.

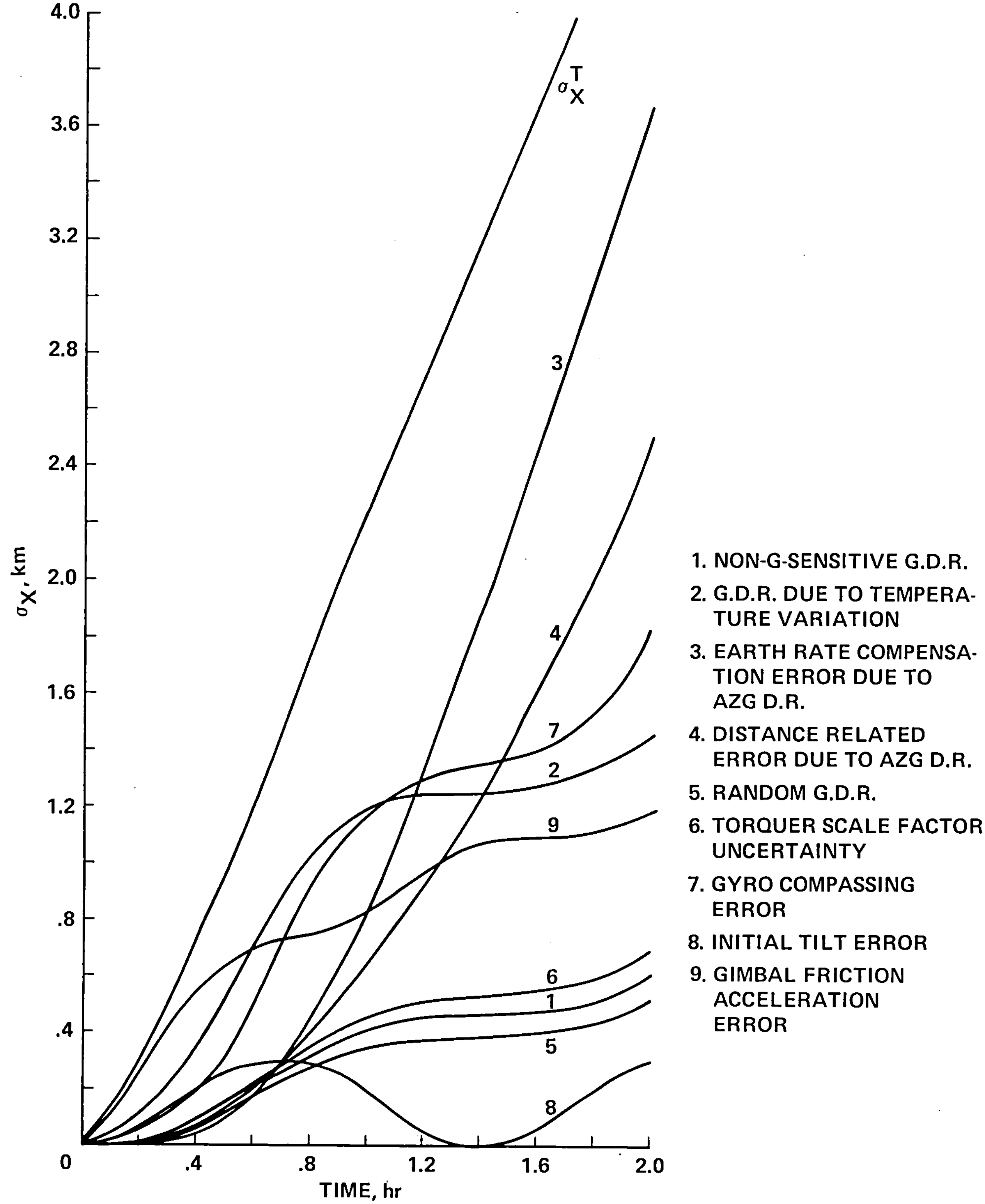

Figure 12.- Positional error propagation with a 25 μrad initial tilt error and constant drift rate of the AZG of $\dot{\psi}_d$ = 0.1°/hr and a stationary random temperature variation of the LEG of 1° F.

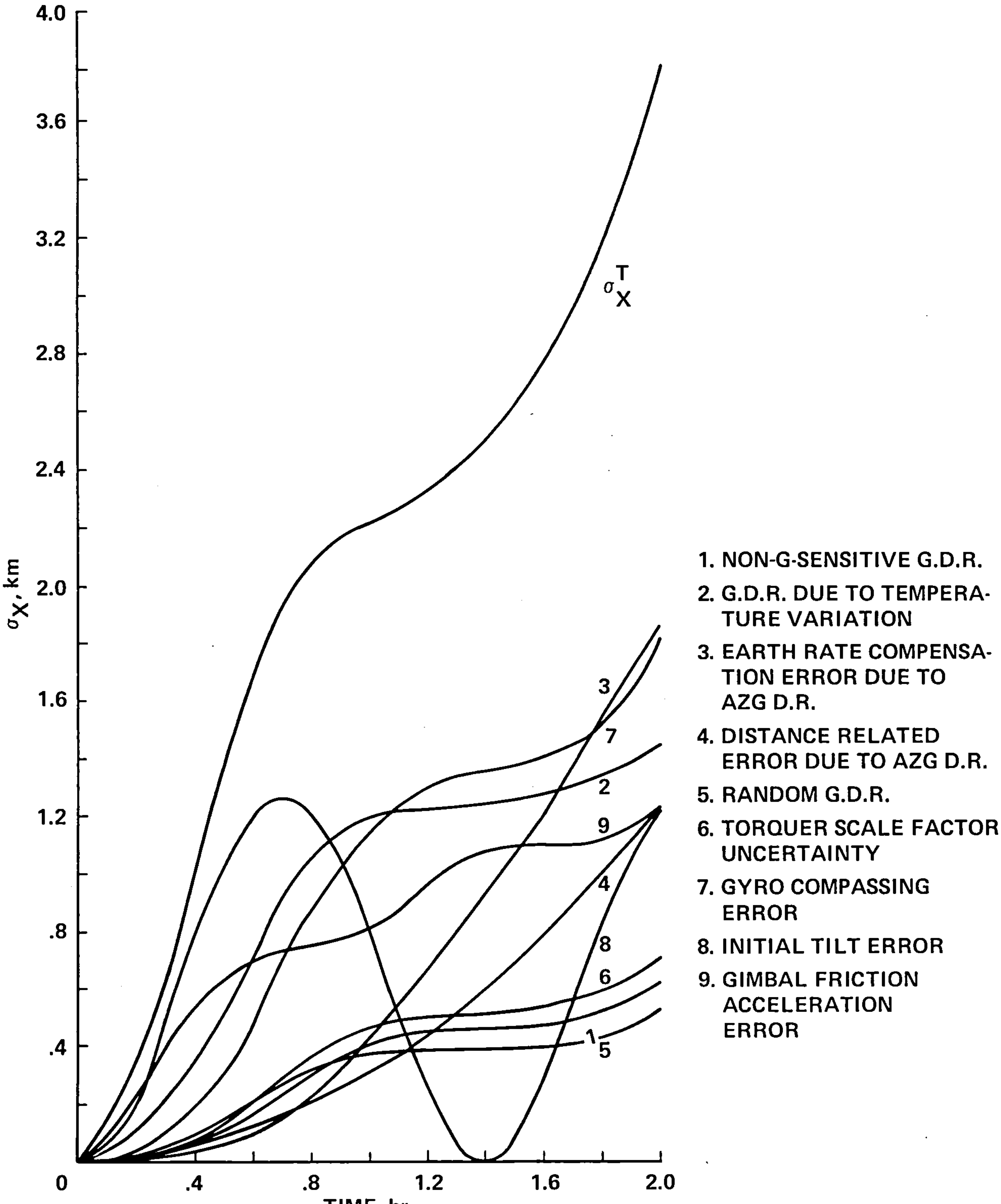

Figure 13.- Positional error propagation with a 100 μrad initial tilt error, a drift rate of the AZG of $\dot{\psi}_d$ = 0.05°/hr, and a stationary random temperature variation of the LEG of 1° F.

1. Report No.	2. Government Accession No.	3. Recipient's Catalog No.
NASA TM-78611		

4. Title and Subtitle	5. Report Date
LOW-COST INERTIAL NAVIGATION FOR MODERATE-g MISSIONS	6. Performing Organization Code
7. Author(s) Shmuel J. Merhav*	8. Performing Organization Report No. A-7920
9. Performing Organization Name and Address Ames Research Center, NASA Moffett Field, Calif. 94035	10. Work Unit No. 505-07-10-02
	11. Contract or Grant No.
12. Sponsoring Agency Name and Address National Aeronautics and Space Administration Washington, D.C. 20546	13. Type of Report and Period Covered Technical Memorandum
	14. Sponsoring Agency Code

15. Supplementary Notes

*Senior NRC Research Associate. Professor, Department of Aeronautical Engineering, Technion, Haifa, Israel.

16. Abstract

This paper describes a low-cost inertial navigation system (INS) concept for a broad class of flight missions characterized by moderate accelerations and limited attitude variations. Typically, these missions may involve general aviation aircraft, helicopters, or remotely piloted vehicles (RPV). Though highly desirable, the use of inertial navigation in these aircraft might be precluded by the high cost of INS technology constituting a substantial fraction of the total aircraft cost. The significance of the moderate acceleration and limited attitude is reviewed with respect to platform mechanization and instrumentation, and a novel hybrid mechanization, partially gimballed and partially strapdown, is presented. Implemented by an unbalanced two-axis gimbal system, controlled by a two-degree-of-freedom gyro, it provides locally level two-axis acceleration information, along with pitch and roll measurement. Heading information is provided by a second gyro mounted in the inner gimbal. It is shown that the system error model is equivalent to that of a conventional platform with a tilt error determined by the integral of the gyro drift rate and an equivalent accelerometer bias proportional to the same drift angle. Thus, by calibrating platform drift rate, the accelerometer-type errors are also cancelled. Rapid gyrocompassing, implemented with opened gimbal control loops, and a strapdown procedure also provides calibration of gyro drift rate biases. Being subjected to small angular inputs and a low-g environment, g and g^2 dependent errors are negligible. Thus, adequate precision can be obtained from moderate cost gyroscopes, resulting in a rms navigation error of the order of 1 n. mi./hr. The dispensing of accelerometers and the simplified mechanization and computation imply substantial cost savings and improvement of reliability.

17. Key Words (Suggested by Author(s))	18. Distribution Statement
Instrumentation Navigation Guidance Control	Unlimited STAR Category - 06

19. Security Classif. (of this report)	20. Security Classif. (of this page)	21. No. of Pages	22. Price*
Unclassified	Unclassified	62	$5.25

*For sale by the National Technical Information Service, Springfield, Virginia 22161